TÜBİTAK

Turkish Journal of Earth Sciences

http://journals.tubitak.gov.tr/earth/

Research Article

Turkish J Earth Sci
(2016) 25: 341-366

doi:10.3906/yer-1507-9

Assimilation and fractional crystallization of foid-bearing alkaline rocks: Buzlukdağ intrusives, Central Anatolia, Turkey

Kıymet DENİZ[1,*], Yusuf Kağan KADIOĞLU[1,2]

[1]Department of Geological Engineering, Faculty of Engineering, Ankara University, Ankara, Turkey
[2]Earth Sciences Application and Research Center, Ankara University, Ankara, Turkey

Received: 15.07.2015 • **Accepted/Published Online:** 06.04.2016 • **Final Version:** 09.06.2016

Abstract: Felsic intrusive rocks within the Central Anatolian Crystalline Complex provide a window into the geodynamic processes in operation during the final closure of the Neotethys Ocean. Previous studies were largely restricted to the calc-alkaline granitoids, and the structural and petrogenetic relations of syenitoids are poorly studied. The Buzlukdağ Intrusive Complex is a silica-undersaturated alkaline syenite that is differentiated into three concentric subgroups according to texture and grain size. Mineral compositions do not vary between the subgroups but differentiation has resulted in different mineral proportions. Mafic microgranular enclaves are present throughout the suite, indicating mingling and mixing between the coeval felsic and mafic magmas. Major element concentrations are consistent with fractional crystallization of nepheline + K feldspar ± Na rich plagioclase + Na amphibole + pyroxene ± melanite ± cancrinite. Mineral chemistry reveals that the syenites are crystallized under a wide range of pressures (1.5–3.7 kbar), at varying temperatures (732–808 °C), and are likely emplaced at depths of 6–14 km. Large-ion lithophile element and light rare earth element enrichments with respect to high field-strength elements and heavy rare earth elements are consistent with their derivation from an incompatible element-enriched magma source. Incompatible trace element concentrations (e.g., Sr, Ba, Th, Ta, Pb, La, Ce, and Yb) revealed that the magma has a subduction fluid component, which can be distinguished from crustal assimilation. The Buzlukdağ alkaline intrusive rocks are likely to be derived from decompressional melting of the lithospheric mantle above asthenospheric upwelling as a result of crustal thinning of Central Anatolia during the Late Mesozoic–Early Cenozoic.

Key words: Buzlukdağ syenite, alkaline rocks, assimilation and fractional crystallization, subduction zone metasomatism, lithospheric mantle, enclave

1. Introduction

Silica-undersaturated alkaline rocks are formed in nearly all tectonic environments with the exception of mid-ocean ridges (Fitton and Upton, 1987). They are formed during oceanic and continental intraplate magmatism and subduction magmatism. Despite this, these rocks comprise volumetrically less amounts of all igneous rocks (Fitton and Upton, 1987). Silica-undersaturated alkaline rocks also point out the areas where crustal thinning is observed in association with continental intraplate magmatism and the partial melting of the deepest and phlogopite-rich part of the subducted plate. However, they attract attention because of their characteristic high concentrations of incompatible, large-ion lithophile elements (LILEs) and rare earth elements (REEs) and their important ore deposits of fluorite, barite, apatite, and diamond (Fitton and Upton, 1987). As a result of a wide range of tectonic occurrences, alkaline igneous rocks are noticed in northwestern Ontario, Greenland, Iceland, Africa, America, Europe, Asia, the Hawaiian Islands, and Russia. Even though the products of alkaline magmatism in Turkey are observed in all areas (northern, western, eastern, and central parts of Anatolia), cropping out in small areas, the alkaline igneous rocks of the northeastern part of Anatolia are located near Ordu (Yenisayaca, İkizce), Trabzon, and Artvin (Pırnallı) (Temizel and Arslan, 2008, 2009; Karsli et al., 2012; Temizel et al., 2012). The alkaline igneous rocks of western Anatolia are mostly located around Kütahya (Seyitgazi, Kırka), Afyon (Şuhut, Sandıklı), Isparta (Gölcük, Bucak), and Manisa (Kula). Adıyaman (Nemrut) and Van (Tendürek) are the areas where alkaline igneous rocks are observed in the eastern part of the Anatolia (Keskin, 2003; Özdemir et al., 2006; Ersoy and Helvacı, 2007; Ersoy et al., 2008, 2010a, 2010b, 2011, 2012; Dilek and Altunkaynak, 2009, 2010). Kırşehir (Akçakent, Bayındır, Buzlukdağ), Kayseri (Hayriye), Nevşehir (Devepınarı, İdişdağ), and Yozgat (Ömerli) are the main locations for central Anatolia (Kadıoğlu et al.,

* Correspondence: kdeniz@eng.ankara.edu.tr

2006). The alkaline volcanic rocks are mostly observed in northeastern, western, and eastern parts, whereas the plutonic equivalents are seen in central parts in the composition of syenites (Figure 1). Buzlukdağ is the best area where these rocks are observed in the Central Anatolia Crystalline Complex (CACC) and the only area where syenites have contact with metamorphic rocks.

The Late Cretaceous igneous rocks of Central Anatolia, Turkey, recorded the magmatic and tectonic evolution of the region during closure of the İzmir-Ankara-Erzincan (İAE) and Inner Tauride (IT) oceans, which constituted the northern branches of the Neotethys Ocean (Şengör and Yılmaz, 1981; Bozkurt and Mittwede, 2001). Syenites are important indicator for reflecting the changes of the tectonic regime from compressional to extensional and the type of tectonic settings (Channel, 1986). Their petrographic and geochemical characteristics have significant importance in understanding mantle activities in the subduction zones and also mantle–crust interactions. Previous geochemical and geochronological studies largely concentrated on the calc-alkaline plutonic rocks (Aydın et al., 1998; Tatar and Boztuğ, 1998, 2005; Boztuğ and Arehart, 2007; Boztuğ and Harlavan, 2008; Boztuğ et al., 2009; Köksal et al., 2012; Elitok et al., 2014). In contrast, there are few comparative studies of the calc-alkaline, transitional, and alkaline igneous rocks with very poor data from alkaline rocks (Boztuğ, 1998, 2000; Otlu and Boztuğ, 1998; Tatar, 2003; İlbeyli, 1999, 2005; İlbeyli et al., 2004, 2009; Köksal et al., 2004; Köksal and Göncüoğlu, 2008) and little emphasis on their importance for the tectonic evolution of the region and ore deposition. The Buzlukdağ Intrusive Complex, which is located in the northwestern part of the CACC, is one of largest silica-undersaturated alkaline bodies and includes syenite, felsic and mafic dykes, and enclaves (Tolluoğlu, 1986, 1993; Kadıoğlu et al., 2006; Deniz, 2010) (Figure 1). The compositional range of rocks present in the complex makes it a good place to study the formation and evolution of the CACC syenitic rocks. The aim of this study is to present a detailed geology map, petrographic investigation of the main lithologies, the relationship between the syenite and dykes, and the mineral and whole-rock major and trace element geochemical characteristics of the Buzlukdağ Intrusive Complex (Deniz, 2010) in order to understand the petrogenesis of the complex, and the comparison with the other alkaline syenitic rocks (İdişdağ, Hayriye, Ömerli, Akçakent, Dumluca, Murmana, Karakeban, Kösedağ, Hasançelebi, Karaçayır, Davulalan, Baranadağ, Bayındır (Hamit), Durmuşlu, Çamsarı) within the CACC.

2. Geological background

The CACC is the microcontinent that is bounded by the İAE Suture Zone dipping northward beneath the Pontides at the north and the IT Suture Zone with NE-dipping

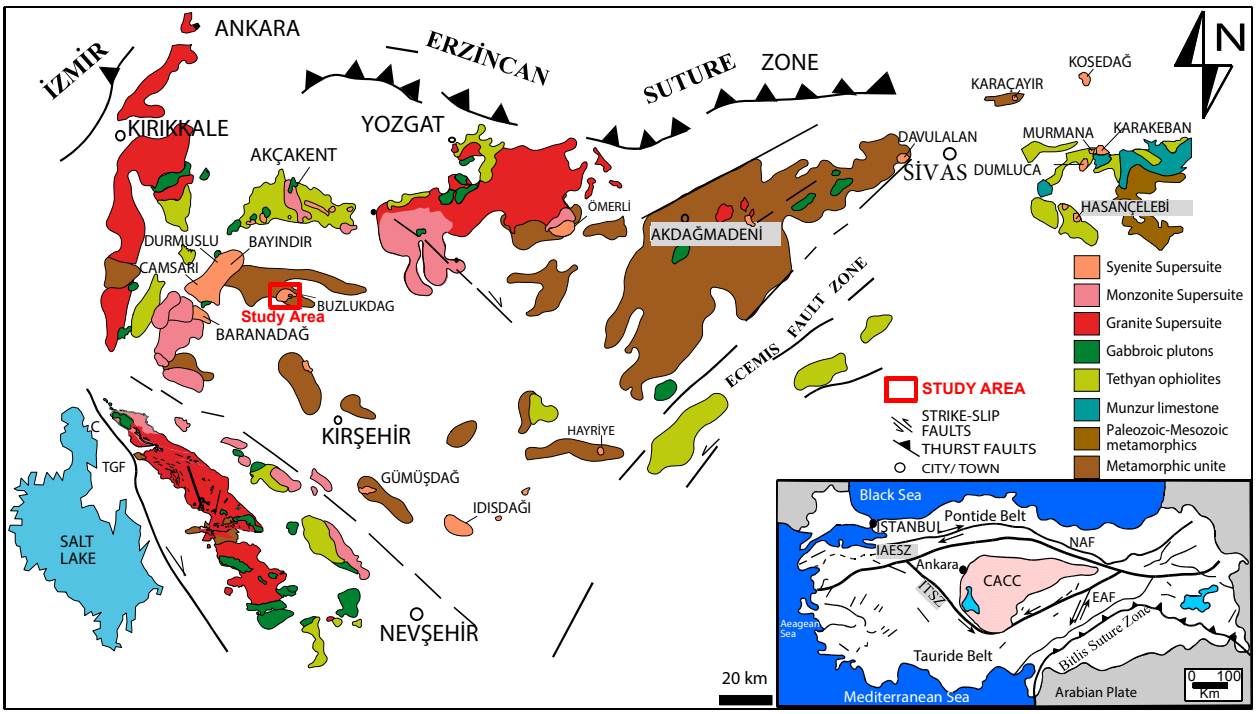

Figure 1. Geological sketch map of the Central Anatolia Crystalline Complex (CACC) modified from Kadıoğlu et al. (2006) with inset map from Bozkurt (2001).

subduction beneath the CACC at the south (Kadıoğlu et al., 2006). The magmatism within the CACC is related to the closure of the IT Ocean, which is the southern strand of the northern branch of the Neotethys between the Tauride Anatolide Platform (TAP) and CACC. These magmatisms produce several distinct suites of felsic and mafic igneous rocks, which intruded into the metamorphic basement during the Middle to Late Cretaceous after the obduction of the suprasubduction zone Tethyan ophiolite emplaced southward along the northern edge of the CACC in Turonian–Santonian times (90–85 Ma) and before the final collision in the Middle Eocene (Whitney et al., 2001; Köksal et al., 2004; Tatar and Boztuğ, 2005; Kadıoğlu et al., 2006; Boztuğ et al., 2007b; Boztuğ and Harlavan, 2008). These suites were classified into different groups according to their different petrological characteristics such as calc-alkaline, subalkaline–transitional, and alkaline or S–I–H (M or hybrid–H)–A-type granitoids (Tarhan, 1985; Boztuğ, 1998, 2000; İlbeyli, 1999; Tatar, 2003; İlbeyli et al., 2004, 2009). Calc-alkaline rocks are mainly observed at the outer part whereas alkaline rocks are exposed in the inner part of the CACC (Kadıoğlu et al., 2006). Alkaline rocks are divided into two groups, namely silica-saturated and silica-undersaturated rocks, based on their mineralogical composition (Otlu and Boztuğ, 1998; Boztuğ, 1998, 2000; İlbeyli, 1999; İlbeyli et al., 2004, 2009). They range in composition from quartz syenite and feldspathoid-bearing syenite to nepheline diorite (Kadıoğlu et al., 2006). Syenitic intrusive rocks have been reported from the Sivas, Yozgat, Kırşehir, Nevşehir, and Kayseri regions (Otlu and Boztuğ, 1998; Boztuğ, 1998, 2000; İlbeyli, 1999, 2005; Tatar, 2003; İlbeyli et al., 2004, 2009; Köksal et al., 2004; Köksal and Göncüoğlu, 2008). Boztuğ (1998) divided the CACC syenites into eastern and western alkaline associations. Felsic and mafic alkaline rocks from the Sivas-Divriği region (eastern association) are derived from two different magma sources that occur from the partial melting of upper mantle material, whereas the others (western association) are the early fractionation derivatives of the same magma source. Unfortunately, there is no consensus about the origin of the alkaline magmatism in the complex. Early studies suggested that the most likely source of magma was silica-poor and volatile-rich (Lünel and Akıman, 1986). Bayhan and Tolluoğlu (1987) studied some silica-oversaturated and -undersaturated syenites and claimed that partial melting of different sources was responsible for the formation of these rocks. Bayhan (1988) suggested that distinct magma sources are responsible for the formation of Kaman region syenites rather than a single parental magma. Özkan and Erkan (1994) reported that silica-undersaturated syenites from the Kayseri region and partial melting of the residual magma of I-type granitoids were responsible for the formation of these rocks. Crustal anatexis was suggested for the formation of syenites in the Nevşehir region (Göncüoğlu et al., 1997), while others considered the lower crust–upper mantle origin for derivation of these rocks (Boztuğ et al., 1994; Boztuğ, 1998; Otlu and Boztuğ, 1998). Most authors suggest a postcollisional geodynamic setting for the syenitic rocks (Boztuğ, 1998, 2000; İlbeyli, 1998, 2005; İlbeyli et al., 2004, 2009; Köksal et al., 2004; Köksal and Göncüoğlu, 2008), whereas Kadıoğlu et al. (2006) prefer a syncollision model.

3. Field description and petrography

3.1. Buzlukdağ syenites

The Buzlukdağ Intrusive Complex is a W–E trending pluton that has intruded into the Paleozoic metamorphics of the Central Anatolian Metamorphic (CAM) Belt (Seymen, 1981; Whitney et al., 2001) (Figure 2a). These contact rocks are mainly schist, gneiss, and marble in composition. It is mainly composed of foid-bearing syenites with lesser amounts of alkali feldspar syenite, diorite porphyry, and microgabbros. Tolluoğlu (1986) simply mapped the intrusive body and reported that the complex settled into the metamorphics as stocks and dykes, and claimed that the main body is syenite in composition whereas the vein rocks are foid-bearing syenite in composition. In this study, the complex, contact rocks and the surrounding lithologies were mapped in detail (Figure 2a and 2b). Contrary to Tolluoğlu (1986, 1993), the whole complex was formed from foid-bearing rock associations. In the pluton, foid-bearing syenite, alkali feldspar syenite, diorite porphyry, microgabbro, and enclaves (xenolithic and mafic microgranular) were distinguished. The core of the pluton is a fine-grained foid-bearing syenite. Medium and coarse-grained syenites crop out along the northern and southern edge of the pluton (Figure 2a). An outer zone of fine crystalline foid-bearing syenite surrounds coarse and medium-grained foid syenite (Figures 2a and 2b). There is little compositional or mineralogical difference between the zones; they are distinguished largely on the basis of grain size. This magmatic difference may suggest that the syenites intruded as more than one pulse in the region. The modal mineralogical classification diagrams of foid-bearing syenites suggest foid syenite and foid monzo syenite based on Streckeisen (1976, 1979) and leucocratic nepheline syenite on the nepheline–alkali feldspar–mafic mineral triangular diagram by Das and Acharya (1996) (Figure 3). It is primarily composed of nepheline, orthoclase, plagioclase (oligoclase and andesine), pyroxene (augite, salite, fasaite), biotite, phlogopite, and amphibole (edenite, ferroedenite, and ferropargasite) with sparse garnet (melanite), cancrinite, nosean, sphene, and opaque minerals (Figures 4a–4c). The fine-grained syenite is extensively altered to illite, smectite, and kaolinite, which are determined by X-ray diffraction (XRD) analyses.

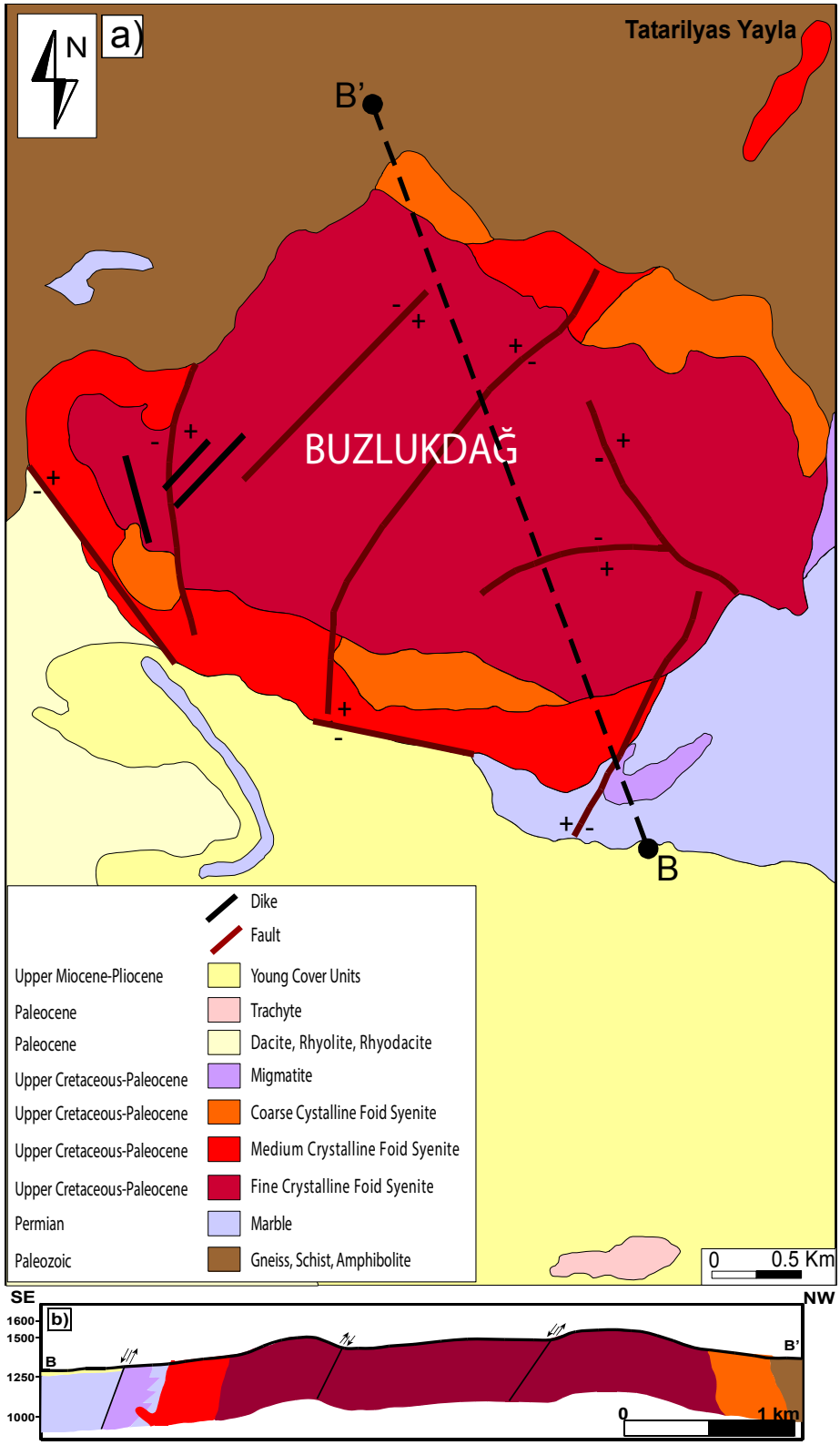

Figure 2. (a) Detailed geological map of Buzlukdağ region. (b) Geological cross-section along B – B'.

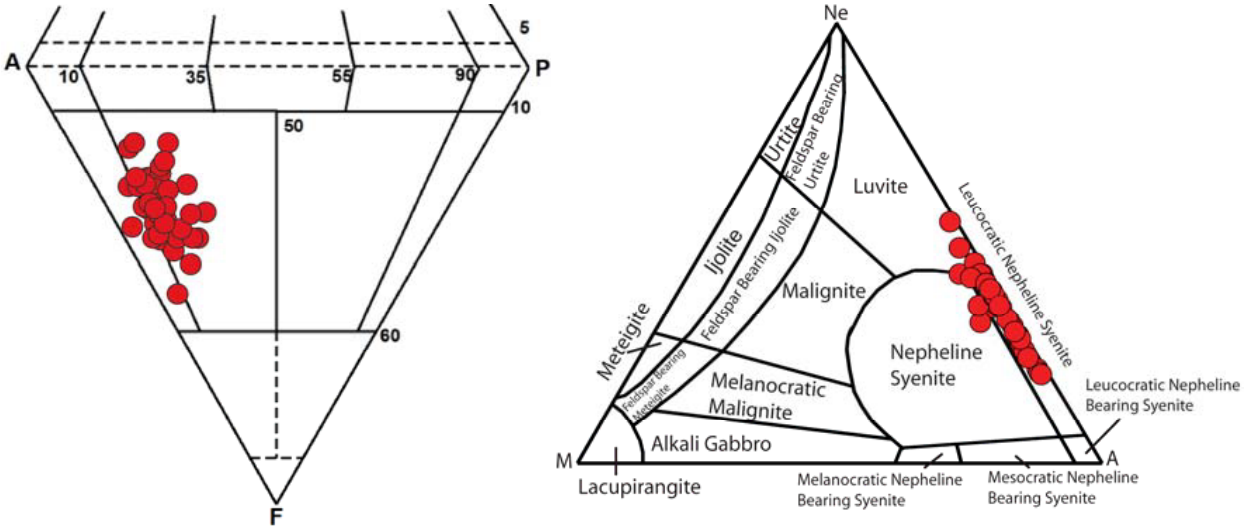

Figure 3. Modal mineralogical compositions and Ne–M–A discrimination of Buzlukdağ syenitoids (Streckeisen, 1976, 1979; Das and Acharya, 1996) (A: alkali feldspar, F: feldspathoid, P: plagioclase; Ne: nepheline, M: mafic minerals).

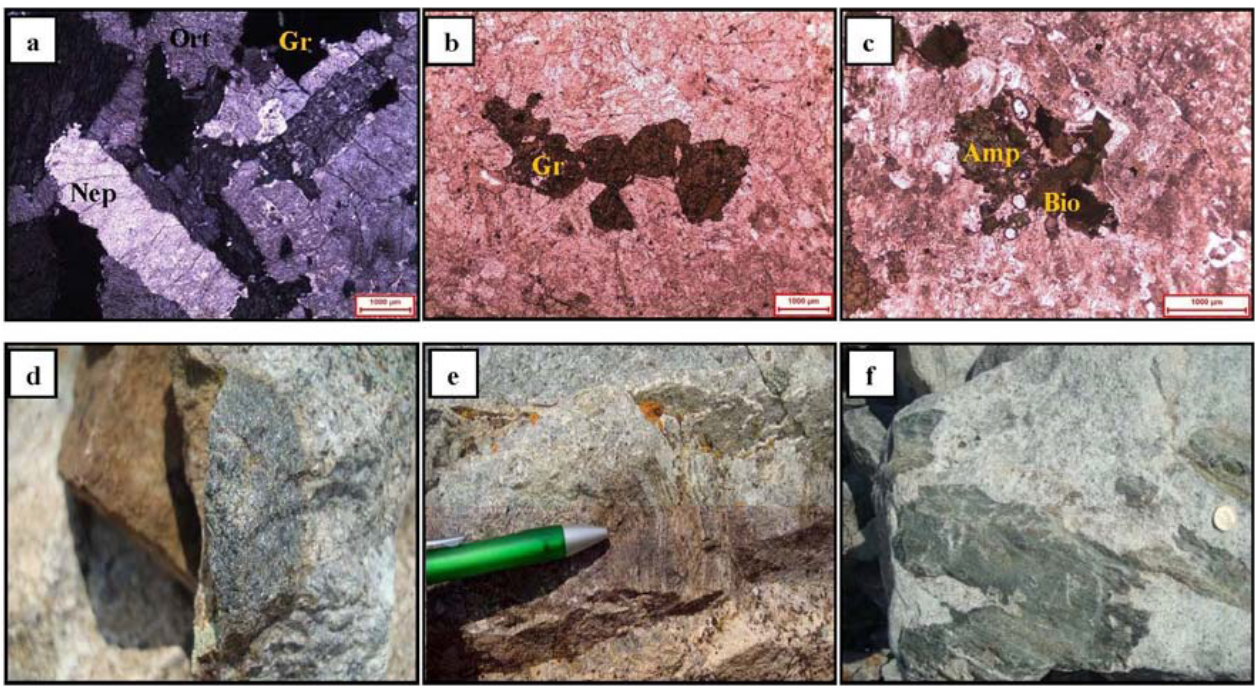

Figure 4. (a, b, c) Photomicrograph of Buzlukdağ syenites, (d) photograph of mafic magmatic enclave, (e, f) photographs of xenolithic enclaves within the Buzlukdağ syenites (Nep: nepheline, Ort: orthoclase, Gr: garnet, Qu: quartz, Amp: amphibole, Bio: biotite).

Where the outer zones of syenites are in contact with the Paleozoic schists, there is extensive migmatite and contact metamorphism, evidenced by hornfels and marble (Figure 2).

The pluton is cut by NE-SW and NW-SE trending normal faults that contain fluorite ± tourmaline mineralization.

3.2. Felsic and mafic dykes

A series of felsic and mafic dykes (up to 15 cm thick), parallel to the main fault trends, cut the fine-grained syenite. The felsic dykes are foid-bearing alkali feldspar microsyenites. They are very fine crystalline and nepheline, orthoclase, and plagioclase are the main mineral assemblages. The mafic dykes are dominantly foid diorite porphyry and

foid gabbro in composition. They are mainly composed of nepheline, plagioclase, pyroxene, ilmenite, and magnetite. They vary in width from 5 to 10 cm.

3.3. Enclaves

The Buzlukdağ Intrusive Complex has a minor amount of magma segregation, mafic microgranular and xenolith types of enclaves. Magma segregation enclaves are formed of pyroxene (augite, diopsite) and amphibole (actinolite and tremolite) minerals, which have similar mafic mineral assemblages with host rock ranging from 100 to 1000 μm. Mafic microgranular enclaves are from 0.5 to 2 cm in size and rarely observed within the syenites (Figure 4d). They are foid diorite and foid monzo diorite in composition and have sharp contact with the host rock. They have an igneous texture and are rich in mafic minerals. These mafic microgranular enclaves represent the mixing and mingling between the felsic and mafic magmas (Yılmaz and Boztuğ, 1994; Kadıoğlu and Güleç, 1996, 1999; Yılmaz Şahin and Boztuğ, 2001). Fine crystalline foid syenites have xenolithic enclaves, which have different mineral compositions and different textural features from the host rock and range from 1 to 15 cm in size (Figures 4e and 4f). Fine crystalline foid syenites have magmatic texture whereas xenolithic enclaves have a metamorphic texture. They have sharp contact with the host rock.

4. Geochemistry

4.1. Analytical methods

After petrographic investigations, mineral chemistry determinations were carried out from the representative samples using a Cameca 100 Superprobe at the Institut für Mineralogie und Mineralische Rohstoffe Technische Universität Clausthal (Germany). A HR-800 (HORIBA-JobinYvon) confocal Raman spectrometer (CRS) was used for identifying the type of pyroxene, mica, and garnet group minerals (Koralay and Kadıoğlu, 2008; Kadıoğlu et al., 2009; Koralay, 2010). XRD analyses were carried out from altered syenite samples using an Inel Equinox 1000 at the laboratory of the Earth Sciences Application and Research Center (YEBİM) of Ankara University.

Major and trace elements were analyzed in whole-rock samples from syenites and felsic and mafic dykes at the laboratory of YEBİM. The concentrations of these elements were determined by polarized energy dispersive X-ray fluorescence (XRF) spectrometer. The instrumentation and preparation procedures were carried out as described in the literature (Kadıoğlu et al., 2009; Koralay, 2010). The REEs were analyzed with an inductively coupled plasma mass spectrometer (ICP-MS) at ACME Laboratories in Canada.

4.2. Mineral chemistry

The compositions of the feldspar, pyroxene, and amphibole group minerals from the Buzlukdağ Intrusive Complex are given in Tables 1–3. The K feldspar plots on the orthoclase region and the plagioclase plot on the andesine and oligoclase regions were determined on the albite–orthoclase–anorthite silicate triangular diagram (Deer et al., 1963) (Figure 5a). Pyroxenes were determined on the core of each crystal and plotted on the salite to fasaite area of the enstatite–wollastonite–ferrosillite triangular diagram (Hess, 1941) (Figure 5b). Amphiboles have (Ca + Na) ≥ 1.34, Na < 0.67 (fine crystalline foid-bearing syenite), and Ca > 1.34 (coarse crystalline foid-bearing syenite). Amphiboles fall into two different fields in the diagram because they have low and high Mg / (Mg + Fe^{+2}) values: edenite/ferro-edenite and pargasite region (Leake, 1978) (Figure 5c). This is probably related to fractional crystallization. According to the hornblende–plagioclase geothermobarometry of Holland and Blundy (1994) and Anderson (1996), it was calculated that foid-bearing syenites were emplaced at 732–808 °C and 1.5–3.7 kbar. This corresponds to an emplacement depth of 5.8–14.2 km assuming an average crustal density of 2650 kg/m^3. Decreasing the alumina contents of the amphibole minerals may cause decreasing pressures values because of the cation exchange during the alteration of these minerals. The wide range of the calculated pressures from different amphiboles might be because of the chloritization of some amphiboles within the rock units.

As a result of CRS studies, the garnets of the foid-bearing syenites are in the composition of andradite (Figure 6a). Foid-bearing syenites mostly contain augite and minor diopsite (Figure 6b). Mica minerals are mostly phlogopite in composition and the iron content is smaller than 0.33 wt.% (Wang et al., 2002) (Figures 6c and 6d).

4.3. Whole-rock geochemistry

SiO_2 contents of silica-saturated and silica-undersaturated alkaline rocks (especially syenites from the Chinduzi, Mongolowe, Chaone, Chikala, Junguni, Chilwa, Velasco, Diablo, and Davis Mountains, etc.) (Woolley and Jones, 1987; Zozulya and Eby, 2008; Eby, 2011) range from 56.3 to 69.0 wt.%. These rocks have Al_2O_3 (13.0–20.9), Fe_2O_3 (0.80–6.33), FeO (1.24–7.50), TiO_2 (0.20–1.67), MnO (0.08–0.27), MgO (0.07–1.90), CaO (0.23–4.58), Na_2O (0.23–9.9), K_2O (3.95–6.68), and P_2O_5 (0.02–0.65) as major element contents (Woolley and Jones, 1987). They have wide ranges of trace element compositions, such as Nb (42–275 ppm), Zr (100–3600 ppm), Y (27–220 ppm), Sr (6–450 ppm), Ba (50–8300 ppm), and Rb (50–350 ppm) (Woolley and Jones, 1987; Zozulya and Eby, 2008; Eby, 2011).

The major and trace element data from foid-bearing syenites and felsic and mafic dykes are given in Table 4. SiO_2 contents range from 57 to 66 wt.% (Figure 7), even though foid-bearing syenites are richer in Fe_2O_3 (up to 5 wt.%) than MgO (0.02 to 0.45 wt.%) (Figure 7). Comparing

Table 1. Representative microprobe analyses of feldspars from the Buzlukdağ syenitoids.

wt.%	32	33	23	24	25	26	27	28	29	30	21
SiO_2	57.83	61.53	58.01	57.93	58.40	57.22	57.72	57.57	56.35	57.06	57.48
TiO_2	0.07	0.00	0.00	1.34	0.80	0.00	0.23	0.00	0.52	0.05	0.05
Al_2O_3	26.20	24.09	26.36	26.23	26.34	26.96	26.86	26.70	27.38	27.02	26.35
FeO	0.14	0.08	0.14	0.16	0.16	0.18	0.15	0.17	0.17	0.15	0.05
MnO	0.00	0.01	0.00	0.00	0.00	0.03	0.01	0.00	0.00	0.00	0.02
MgO	0.00	0.00	0.00	0.00	0.00	0.00	0.00	0.00	0.01	0.00	0.01
CaO	8.22	5.68	8.04	7.77	8.02	9.03	8.52	8.62	9.24	8.92	8.27
Na_2O	6.83	8.49	7.09	7.04	7.20	6.65	6.87	6.68	6.41	6.48	7.03
K_2O	0.13	0.15	0.20	0.20	0.17	0.20	0.17	0.17	0.28	0.21	0.17
Total	99.40	100.05	99.84	100.67	101.10	100.27	100.53	99.91	100.35	99.90	99.44
Numbers of ions on the basis of 32 O											
Si	10.413	10.930	10.404	10.315	10.430	10.256	10.301	10.332	10.111	10.254	10.364
Ti	0.009	0.000	0.000	0.179	0.000	0.000	0.031	0.000	0.070	0.007	0.007
Al	5.560	5.044	5.572	5.504	5.544	5.695	5.650	5.647	5.790	5.723	5.599
Fe	0.021	0.012	0.021	0.024	0.024	0.027	0.022	0.026	0.026	0.023	0.008
Mn	0.000	0.002	0.000	0.000	0.000	0.005	0.002	0.000	0.000	0.000	0.003
Mg	0.000	0.000	0.011	0.011	0.000	0.000	0.000	0.000	0.003	0.000	0.003
Ca	1.586	1.081	1.545	1.482	1.535	1.734	1.629	1.658	1.776	1.718	1.598
Na	2.385	2.924	2.465	2.430	2.493	2.311	2.377	2.324	2.230	2.258	2.458
K	0.030	0.034	0.046	0.045	0.039	0.046	0.039	0.039	0.064	0.048	0.039
$CaAl_2Si_2O_8$	39.64	26.76	38.07	37.45	37.72	42.37	40.26	41.22	43.64	42.67	39.00
$NaAlSi_3O_8$	59.61	72.38	60.80	61.39	61.33	56.52	58.76	57.79	54.80	56.11	60.03
$KAlSi_3O_8$	0.75	0.85	1.13	1.16	0.95	1.11	0.98	0.98	1.55	1.22	0.97

Table 1. (Continued).

	11	31	32	33	34	35	36	37	38	39	40	41
SiO_2	64.27	64.15	63.73	64.91	64.22	64.01	64.47	64.65	64.84	64.45	63.81	64.29
TiO_2	0.00	0.00	0.00	0.03	0.00	0.00	0.00	0.00	0.00	0.00	0.00	0.01
Al_2O_3	18.85	18.41	18.54	18.57	18.48	18.39	18.64	18.63	18.52	18.70	18.54	18.58
FeO	0.08	0.02	0.11	0.10	0.09	0.08	0.07	0.06	0.03	0.07	0.06	0.09
MnO	0.00	0.00	0.04	0.01	0.00	0.01	0.01	0.00	0.04	0.10	0.01	0.02
MgO	0.00	0.00	0.01	0.00	0.01	0.01	0.01	0.00	0.00	0.00	0.01	0.02
CaO	0.03	0.04	0.01	0.00	0.00	0.00	0.00	0.00	0.00	0.01	0.00	0.00
Na_2O	1.47	0.42	0.78	1.86	1.16	0.47	0.67	0.75	1.33	0.71	0.58	0.72
K_2O	14.76	16.25	15.57	13.92	15.09	16.16	15.75	15.97	14.80	15.68	16.11	15.74
Total	99.47	99.28	98.78	99.40	99.06	99.12	99.62	100.05	99.56	99.73	99.11	99.47
Numbers of ions on the basis of 32 O												
Si	11.901	11.958	11.921	11.975	11.951	11.952	11.947	11.945	11.978	11.935	11.920	11.939
Ti	0.000	0.000	0.000	0.004	0.000	0.000	0.000	0.000	0.000	0.000	0.000	0.002

Table 1. (Continued).

Al	4.114	4.044	4.088	4.038	4.053	4.046	4.071	4.056	4.033	4.081	4.083	4.067
Fe	0.013	0.003	0.017	0.016	0.014	0.013	0.011	0.010	0.005	0.011	0.009	0.015
Mn	0.000	0.001	0.006	0.001	0.000	0.002	0.001	0.000	0.006	0.015	0.001	0.003
Mg	0.000	0.000	0.001	0.000	0.003	0.002	0.003	0.000	0.000	0.000	0.002	0.005
Ca	0.006	0.008	0.001	0.000	0.000	0.000	0.001	0.000	0.000	0.002	0.001	0.000
Na	0.528	0.150	0.284	0.664	0.420	0.169	0.240	0.269	0.478	0.256	0.208	0.261
K	3.487	3.864	3.714	3.275	3.582	3.850	3.725	3.764	3.489	3.705	3.840	3.729
$CaAl_2Si_2O_8$	0.16	0.20	0.04	0.00	0.00	0.00	0.01	0.00	0.00	0.06	0.01	0.00
$NaAlSi_3O_8$	13.12	3.73	7.10	16.86	10.50	4.21	6.05	6.66	12.05	6.46	5.15	6.53
$KAlSi_3O_8$	86.72	96.07	92.86	83.14	89.50	95.79	93.94	93.34	87.95	93.48	94.84	93.47

major element compositions with especially silica-undersaturated syenitic rocks from around the world, the Buzlukdağ foid-bearing syenites have higher K_2O and lower TiO_2 contents than other syenites from the literature (Figure 7). The Fe_2O_3 and MgO contents of the Buzlukdağ intrusive rocks (apart from some of the samples) do not display any clear negative or positive trends with increase in the silica content with respect to other alkaline suites from the world (Figure 7). These narrow range variations may be related to the proportion of the mafic minerals within the rocks (Figure 7). Regarding the mafic mineral proportion, there is a similar relation with the MnO and TiO_2 contents in all the alkaline suites except the Chinduzi, Mongolowe, Chaone, Chikala, and Junguni syenitic rocks (Figure 7). There is a significant negative trend in the Al_2O_3 against SiO_2 diagram of the Buzlukdağ intrusive rocks and they have higher Al_2O_3 content (up to 27 wt.%) than the other alkaline suites. Some of the samples from Buzlukdağ syenites show negative trends in Na_2O with increasing SiO_2 content; on the other hand, the other samples do not have a wide range of Na_2O content that is compatible with the other alkaline suites (Figure 7). The Buzlukdağ alkaline intrusive rocks display a wide range of K_2O content (Figure 7).

The foid-bearing syenites and all the other alkaline plutonic rocks plot in the A-type granitoid field of Whalen et al. (1987) (Figure 8) yielding weak alkaline major element compositions (Figure 9a). In the ($Na_2O+K_2O–CaO$) versus SiO_2 discrimination diagram of Frost et al. (2001), they are alkali-rich syenites (Figure 9b), except some of the samples that fall on both field and total Fe-number [FeO/(total FeO+MgO)] versus SiO_2 discrimination diagrams, plotting on the ferroan field (Frost et al., 2001) (Figure 9c). In contrast, most of the other alkaline rocks plot on both the ferroan and magnesian fields (Figure 9c). Some of the samples that plot on the magnesian field result from Mg-rich mafic mineral occurrence within these rocks.

REE data are given in Table 5 and shown in Figure 10. The mid-ocean ridge basalt (MORB)-normalized elemental patterns of trace elements reveal enrichment in LILEs with respect to high field-strength elements (HFSEs) (Figure 10a). Depletions in P and Ti (Figure 10a) suggest that the magmas are formed in part by fractional crystallization from mafic parental magmas (P fractionates into apatite, Ti into Fe–Ti oxides; Thompson et al., 1984).

The foid-bearing syenites and felsic and mafic dykes show enrichments in light rare earth elements (LREEs) with respect to heavy rare earth elements (HREEs). Negative Gd anomaly in some samples is related to F content (fluorite mineral) within the rocks (Figure 10b) (Koç et al., 2003). On the contrary, negative Eu anomalies in the A-type granitoids and Buzlukdağ syenites do not show negative Eu anomalies. This may be because of postmagmatic redistribution of elements by F and/or CO_2-rich hydrothermal fluids (Eby, 2006). Negative Eu anomalies in the A-type granitoids were explained by feldspar fractionation. Silica-undersaturated Buzlukdağ syenites are nepheline normative so feldspars were not the dominant mineral phase.

The major, trace element, and REE chemistries of the felsic and mafic dykes are compatible with the foid-bearing syenites. Trace element and REEs are more enriched in the foid-bearing syenites than in either type of dyke (Figure 10).

5. Discussion

There are still arguments about the origin and importance of these alkaline rocks as to whether they are derived from crustal thickening by the postcollisional or the crustal thinning related to syncollisional events. Geological mapping and mineralogical, petrographic, mineral, and whole-rock geochemical data indicate the same coeval magma source for foid-bearing syenites and dykes in the genesis of the Buzlukdağ Intrusive Complex. The most

Table 2. Representative microprobe analyses of amphiboles from the Buzlukdağ syenitoids.

wt.%	44	38	39	40	41	42	43	11	12	13	14	15
SiO_2	36.28	36.67	36.39	37.09	35.02	35.05	34.32	42.41	35.69	43.85	44.35	43.44
TiO_2	2.27	1.28	3.54	1.44	2.61	1.38	1.88	1.53	2.86	1.35	1.08	3.51
Al_2O_3	13.83	13.45	13.42	12.68	13.32	14.87	14.74	9.38	13.92	8.19	8.23	8.39
FeO	24.92	25.10	25.34	23.75	24.14	25.96	25.54	20.71	22.69	19.96	19.54	19.74
MnO	0.73	0.74	0.83	0.63	0.68	0.74	0.75	0.63	0.44	0.62	0.63	0.60
MgO	4.30	4.64	4.59	6.04	4.77	3.79	3.82	8.33	9.93	9.41	9.47	9.68
CaO	11.20	11.34	11.29	11.53	12.84	11.38	11.23	11.69	0.00	11.59	11.70	11.55
Na_2O	1.67	1.65	1.68	1.55	1.54	1.51	1.40	1.42	0.06	1.32	1.40	1.51
K_2O	3.08	3.08	3.02	3.13	3.00	3.20	3.31	1.29	9.44	1.06	0.94	1.03
Total	98.28	97.94	100.10	97.84	97.92	97.87	96.99	97.39	95.03	97.34	97.34	99.45
Numbers of ions on the basis of 23 O												
Si	5.800	5.886	5.724	5.924	5.651	5.672	5.610	6.560	5.841	6.731	6.784	6.533
Ti	0.273	0.155	0.419	0.173	0.316	0.168	0.231	0.179	0.352	0.156	0.125	0.397
Al	2.606	2.544	2.489	2.387	2.533	2.835	2.839	1.710	2.686	1.483	1.483	1.488
Fe^{+2}	3.332	3.369	3.333	3.172	3.257	3.513	3.491	2.678	3.106	2.562	2.500	2.482
Mn	0.099	0.100	0.110	0.085	0.092	0.101	0.104	0.082	0.062	0.081	0.082	0.077
Mg	1.024	1.111	1.075	1.437	1.147	0.913	0.932	1.921	2.422	2.153	2.160	2.170
Ca	1.918	1.951	1.902	1.974	2.220	1.972	1.966	1.937	0.000	1.906	1.917	1.860
Na	0.516	0.512	0.513	0.480	0.481	0.472	0.443	0.426	0.018	0.393	0.414	0.439
K	0.629	0.631	0.606	0.637	0.617	0.660	0.691	0.254	1.970	0.207	0.184	0.197
OH	2.00	2.00	2.00	2.00	2.00	2.00	2.00	2.00	2.00	2.00	2.00	2.00
	16	17	18	5	6	7	8	9	10	11	12	13
SiO_2	43.58	43.95	42.56	44.71	45.94	44.96	44.57	44.36	44.59	44.53	44.88	45.75
TiO_2	0.81	1.47	1.50	0.93	1.15	1.22	1.22	0.89	1.15	1.05	0.88	1.01
Al_2O_3	8.75	8.55	8.36	7.95	7.23	7.86	7.97	7.90	7.92	7.81	7.94	8.02
FeO	20.49	19.72	19.56	17.26	16.70	17.45	17.78	17.72	17.83	17.99	17.80	15.89
MnO	0.56	0.65	0.63	0.61	0.64	0.65	0.64	0.59	0.54	0.52	0.53	0.55
MgO	8.77	9.49	9.43	11.40	11.89	11.32	11.32	11.47	11.35	11.30	11.20	12.36
CaO	11.24	11.53	11.29	12.09	11.99	12.04	11.82	11.99	12.04	11.95	11.75	11.91
Na_2O	1.49	1.45	1.40	1.55	1.44	1.57	1.55	1.46	1.48	1.50	1.59	1.63
K_2O	1.08	1.11	1.09	1.15	0.92	1.07	1.09	1.17	1.06	1.04	1.06	1.08
Total	96.78	97.92	95.83	97.65	97.89	98.13	97.96	97.54	97.96	97.67	97.63	98.20
Numbers of ions on the basis of 23 O												
Si	6.740	6.699	6.647	6.765	6.886	6.769	6.734	6.737	6.738	6.752	6.793	6.815
Ti	0.095	0.169	0.176	0.106	0.129	0.138	0.139	0.102	0.131	0.120	0.101	0.113
Al	1.594	1.536	1.538	1.418	1.277	1.394	1.419	1.413	1.410	1.395	1.416	1.408
Fe^{+2}	2.650	2.514	2.556	2.183	2.094	2.197	2.247	2.250	2.253	2.281	2.254	1.979
Mn	0.074	0.084	0.084	0.078	0.081	0.083	0.082	0.075	0.069	0.066	0.067	0.069
Mg	2.023	2.157	2.197	2.572	2.656	2.540	2.551	2.598	2.557	2.554	2.527	2.744
Ca	1.863	1.883	1.889	1.961	1.926	1.942	1.914	1.951	1.950	1.942	1.906	1.901
Na	0.447	0.427	0.423	0.454	0.419	0.457	0.455	0.429	0.432	0.441	0.467	0.471
K	0.212	0.216	0.218	0.221	0.175	0.206	0.210	0.226	0.205	0.201	0.205	0.205
OH	2.00	2.00	2.00	2.00	2.00	2.00	2.00	2.00	2.00	2.00	2.00	2.00

Table 3. Representative microprobe analyses of pyroxenes from the Buzlukdağ syenitoids.

wt.%	33	34	35	36	37	24	25	26	23
SiO_2	46.61	47.82	45.55	44.69	44.77	46.61	50.78	50.75	28.79
TiO_2	1.35	1.06	1.93	1.60	1.63	1.35	0.70	2.73	33.79
Al_2O_3	6.93	5.57	7.67	8.84	8.57	6.93	1.81	1.82	1.89
FeO	9.23	8.89	10.13	11.61	12.45	9.23	10.53	10.79	2.14
MnO	0.21	0.15	0.21	0.29	0.38	0.21	0.67	0.65	0.09
MgO	11.40	12.44	10.22	9.03	8.42	11.40	11.93	11.44	0.06
CaO	23.75	24.30	23.34	22.95	22.86	23.75	23.14	23.74	27.39
Na_2O	0.58	0.51	0.92	0.91	1.03	0.58	0.55	0.49	0.08
K_2O	0.01	0.00	0.00	0.00	0.02	0.01	0.00	0.01	0.00
Total	100.08	100.74	99.96	99.92	100.13	100.08	100.11	102.44	94.24
Numbers of ions on the basis of 6 O									
Si	1.765	1.796	1.737	1.715	1.723	1.765	1.925	1.887	1.207
Ti	0.038	0.030	0.055	0.046	0.047	0.038	0.020	0.076	1.065
Al	0.310	0.247	0.345	0.400	0.389	0.310	0.081	0.080	0.093
Fe	0.292	0.279	0.323	0.373	0.401	0.292	0.334	0.336	0.075
Mn	0.007	0.005	0.007	0.009	0.012	0.007	0.021	0.021	0.003
Mg	0.644	0.696	0.581	0.517	0.483	0.644	0.674	0.634	0.004
Ca	0.964	0.978	0.954	0.944	0.942	0.964	0.940	0.946	1.230
Na	0.042	0.037	0.068	0.068	0.077	0.042	0.041	0.036	0.007
K	0.001	0.000	0.000	0.000	0.001	0.001	0.000	0.001	0.000
Wollastonite	56.32	55.98	57.80	58.37	58.81	56.32	51.01	50.55	93.96
Enstatite	37.62	39.86	35.23	31.96	30.15	37.62	36.61	33.89	0.30
Ferrosillite	6.06	4.16	6.97	9.67	11.04	6.06	12.38	15.56	5.74

important points are the crystallization processes, which modify the composition of magma during solidification, and the origin of the magma sources in the genesis of the silica-undersaturated syenites of the Buzlukdağ Intrusive Complex. All of these will be discussed in this research.

5.1. Fractional crystallization

Boztuğ (1998) reported fractional crystallization (FC) using whole-rock geochemistry for most of the alkaline, silica-oversaturated, and silica-undersaturated alkaline rocks, which do not include Buzlukdağ pluton.

Major and trace element and REE data are used to illustrate the effect of FC on the evolution of the syenites. As seen in Figure 7, there are not very clear differentiation trends in most of the Harker variation diagrams. Samples from Buzlukdağ syenites show positive trends for Fe_2O_3, MnO, TiO_2, MgO, P_2O_5, and CaO whereas Al_2O_3 concentration has a negative trend against SiO_2. The concentrations of K_2O, Na_2O, and MgO display both negative and positive correlations with increasing silica content.

The low MgO content indicates that they are not primary magma compositions. The magmas from which these rocks are derived are exposed to significant FC within the magma chamber. Na_2O and K_2O partially decrease with increased differentiation because of nepheline, K feldspar, and Na-rich plagioclase fractionation. Decrease in Al_2O_3 content is also related to mineral crystallization. CaO increases with SiO_2, indicating Na-rich plagioclase fractionation. The increases in Fe_2O_3, MgO, and TiO_2 with respect to SiO_2 concentrations indicate that the felsic mineral phases are dominant in the crystallization assemblage during FC of these rocks (Figure 7).

Trace element patterns are similar. Depletion in Sr and Ba reflect the control of feldspar group minerals (plagioclase and alkali feldspar, respectively). Positive trends in Th represent enrichment of crustal materials with FC. Negative Ti and P anomalies are related to sphene and apatite fractionation, respectively. Negative Y anomaly is related to amphibole fractionation and Hf anomaly probably illustrates the occurrence of sphene (Figure 10).

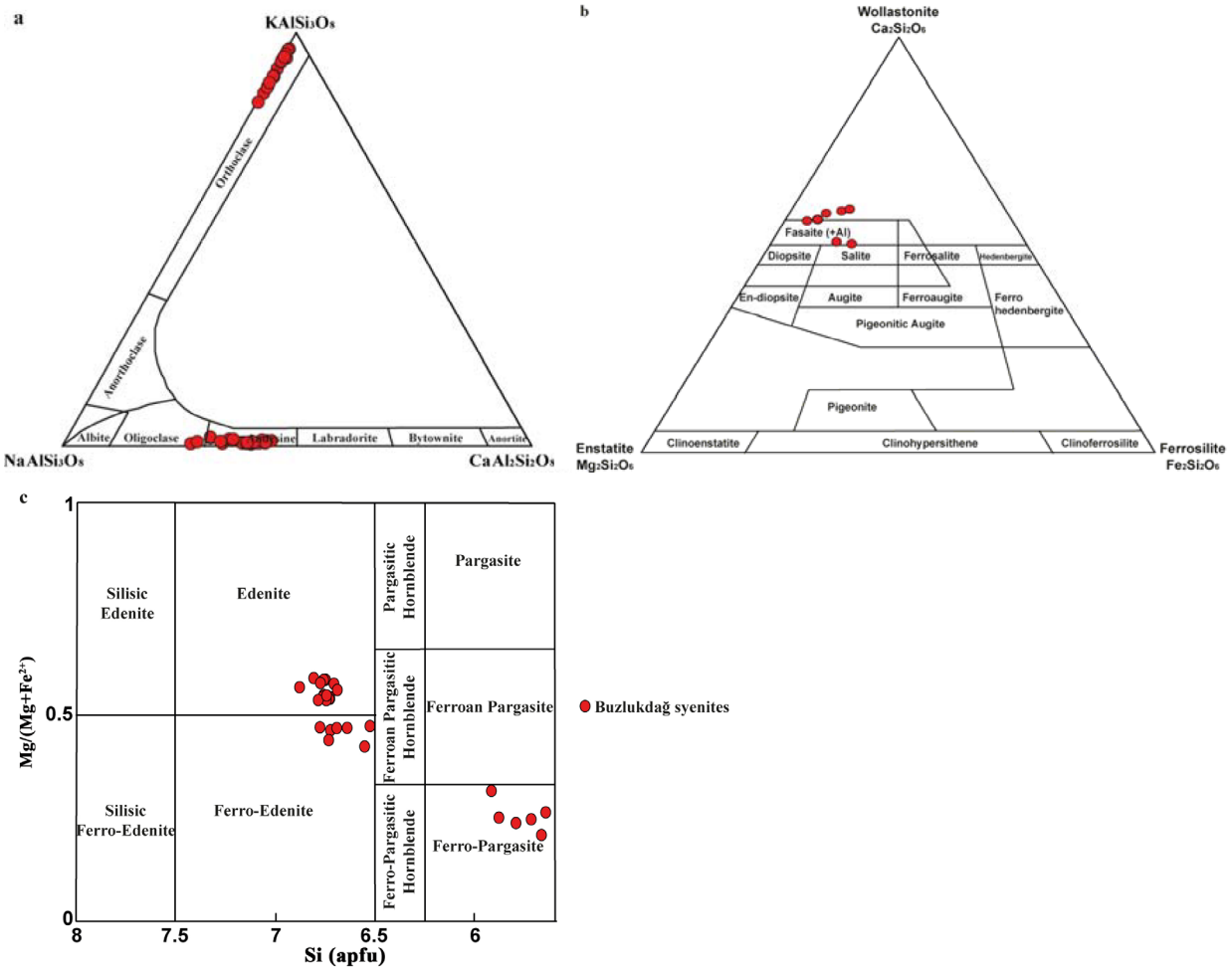

Figure 5. Compositions of feldspars (a), clinopyroxene (b), and amphiboles (c) in the Buzlukdağ intrusives (Hess, 1941; Deer et al., 1963; Leake, 1978).

5.2. Assimilation and fractional crystallization

Alkaline magmatic rocks occupy small outcrops in comparison to calc-alkaline magmatic rocks within Central Anatolia. The mineralogical and geochemical features have a significant role in the interpretation of the nature of the magmatic intrusion in the region, so determining the processes that modify the primary composition of alkaline magma is very important.

İlbeyli (1999, 2005) reported assimilation combined with fractional crystallization (AFC), which modified the composition of magma during crystallization on the basis of well-defined major and trace element variations from one of the alkaline plutons that consists of both silica-oversaturated and silica-undersaturated rocks.

Trace element variation diagrams for some alkaline plutons from around the world are presented in this study. According to the log Th/Yb–log Ta/Yb diagram (Pearce, 1983), the Buzlukdağ syenites and other alkaline suites plot upward from the enriched mantle array and follow the AFC trend (Figure 11a). Buzlukdağ intrusive rocks have higher Th content, which is a subduction-derived element, than other alkaline rocks. Similar relations can be seen in Figure 11b; all alkaline intrusive rocks form trends that run parallel to the mantle metasomatism array but are displaced towards higher Th/Y and Nb/Y ratios, suggesting that they are either derived from an enriched mantle source, to which a subduction component had been added, or coupled crustal contamination with fractional crystallization, or both.

5.3. Source characteristics

A-type granitoids are subaluminous or peralkaline, anhydrous rocks that are formed in anorogenic settings (Eby, 1992, 2006, 2011). The water content of the magma affects the silica saturation of the products of this magma. Bonin (1987, 1988, 1990) suggests the importance of water (H_2O) efficiency in the magma chamber during the solidification process. Water efficiency affects the silica saturation in alkaline rocks (Bonin, 1987, 1988, 1990).

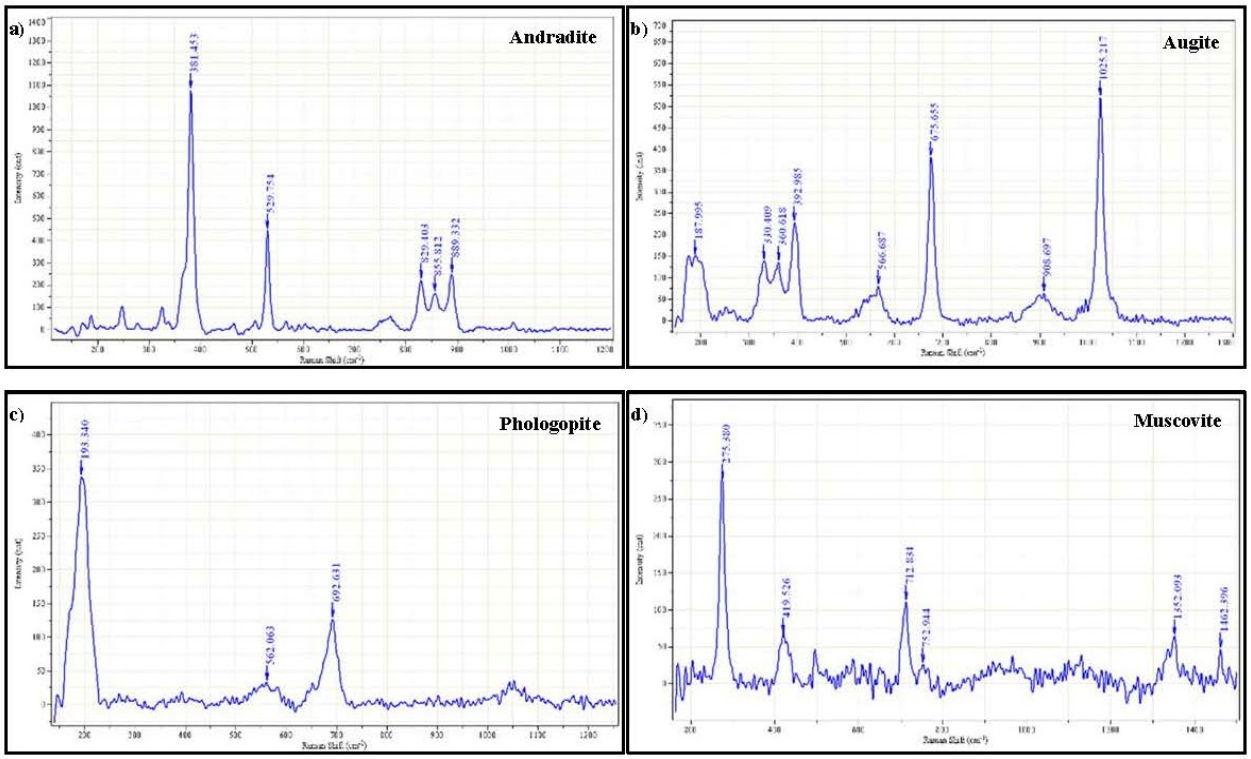

Figure 6. Raman spectra of the (a) andradite, (b) augite, (c) phlogopite, and (d) muscovite minerals.

Primary alkaline magmas are derived from water deficiency and low-degree partial melting of the upper mantle source (Bonin, 1988; McKenzie and Bickle, 1988). During the solidification of these primary magmas within the crust, the water content of wall rocks and the diffusivity of water from these rocks change the composition of the magma chamber and these affect the diversification of alkaline magma. If the wall rocks have high water content, silica-oversaturated alkaline rocks are derived from the magma (Bonin, 1987, 1988, 1990). On the contrary, as mentioned above, the different types and degrees of partial melting of the source material have roles in the genesis of alkaline magma (Wilson, 1989; Rollinson, 1993; Albaréde, 1996). Buzlukdağ intrusives intruded into the metamorphic rocks that have low water content and because of that silica-oversaturated rocks are not seen at Buzlukdağ. Buzlukdağ is the only area where alkaline intrusives intruded into the metamorphic rocks within the CACC. Having high LILE/HFSE concentrations cannot be explained by only FC, the crustal contamination, or both, so these are also ascribed to the addition of LILE-enriched, Nb–Ta-poor fluid components to the mantle wedge, or primary retaining of Nb–Ta in amphibole relative to other phases in the mantle source (Nelson and Davidson, 1993; Pearce and Parkinson, 1993; Pearce and Peate, 1995; Hawkesworth et al., 1997; Zellmer et al., 2005). The diagrams of trace element ratios may be useful indicators for defining these processes. Buzlukdağ intrusive rocks and other alkaline plutons do not display only one trend in the SiO_2 versus Ba/Nb diagram (Figure 12a). All the samples show both FC and crustal contamination trends as in Figure 11. Trace element ratio diagrams may be more useful because of their behavior during the crystallization processes rather than using Ba, which is more related to the FC process. In Figure 11, there is involvement of an incompatible element enriched component in the source of all alkaline rocks. These trends suggest either derivation from an enriched mantle source to which a subduction component had been added, or coupled crustal contamination with FC, or both. These kinds of rocks are derived from sources metasomatized by a fluid component, from sources enriched by bulk sediments and partial or bulk melt of subducted sediments (Hawkesworth et al., 1997; Elburg et al., 2002). In order to define the source of the metasomatism, Th/La versus Ce/Pb, Sr/La versus La/Yb, and Th/Yb versus Ba/La trace element ratio variation diagrams were used. As seen in Figure 12b, there is no trend in the Buzlukdağ intrusive rocks but slab fluid metasomatism was affected by the sources of all alkaline rocks rather than the subduction sediment (Figures 12c and 12d). According to all this theoretical and analytical information, the Buzlukdağ Intrusive Complex may

Table 4. Representative major (wt.%) and trace element (ppm) compositions of the Buzlukdağ syenitoids.

Sample no.	Fine crystalline nepheline syenite						
	BUZ-101	BUZ-102	BUZ-104	BUZ-105	BUZ-107	BUZ-108	BUZ-112
SiO_2	64.98	65.63	59.46	60.92	62.38	65.33	65.10
Al_2O_3	15.55	14.84	24.50	23.54	20.96	15.93	18.76
Fe_2O_3	2.55	2.73	1.46	1.35	1.66	2.65	0.59
MgO	0.50	1.07	0.03	0.09	0.29	0.28	0.03
MnO	0.17	0.17	0.05	0.18	0.12	0.23	0.05
Na_2O	5.07	5.12	3.86	5.10	5.66	3.12	5.25
K_2O	7.60	6.42	7.72	6.94	6.32	9.72	8.05
CaO	2.17	2.66	0.29	0.17	0.84	1.45	1.10
TiO_2	0.20	0.26	0.05	0.06	0.13	0.05	0.02
LOI	0.75	0.70	2.16	1.39	1.24	0.77	0.91
Total	99.90	99.94	99.64	99.82	99.75	99.86	99.92
Ga	21.70	21.00	31.60	30.80	26.10	25.10	33.20
Rb	333.50	319.80	379.00	325.50	293.70	387.70	417.50
Sr	685.10	698.90	301.60	470.40	594.20	732.80	195.90
Y	11.10	21.30	1.20	1.20	1.20	7.30	1.30
Zr	322.20	947.00	120.80	194.30	199.80	263.10	138.20
Nb	40.10	56.70	62.90	38.80	124.30	42.10	30.80
Ba	1444.00	1757.00	680.00	613.10	740.00	2118.00	204.80
Ce	165.40	212.50	191.90	398.80	353.70	204.40	61.00
Hf	3.80	16.20	2.50	3.10	3.70	5.00	3.90
Ta	3.40	2.70	4.30	3.30	2.90	2.90	2.90
Th	35.70	41.80	27.30	59.70	38.00	86.70	8.10
Sample no.	Fine crystalline nepheline syenite						
	BUZ-125	BUZ-126	BUZ-127	BUZ-17	BUZ-19	BUZ-26	BUZ-28
SiO_2	59.98	64.72	60.98	65.78	65.20	65.06	64.94
Al_2O_3	23.73	17.56	22.60	17.14	16.73	18.22	16.99
Fe_2O_3	1.77	2.17	1.64	1.92	2.13	1.84	2.38
MgO	0.13	0.03	0.03	0.13	0.07	0.08	0.37
MnO	0.12	0.04	0.07	0.03	0.05	0.07	0.08
Na_2O	6.14	5.72	7.67	6.27	6.15	6.06	5.49
K_2O	4.51	6.79	2.76	6.36	6.39	7.10	6.78
CaO	1.30	0.93	2.00	1.00	1.49	0.48	1.81
TiO_2	0.10	0.17	0.09	0.23	0.23	0.20	0.15
LOI	1.76	1.70	1.84	0.86	1.18	0.75	0.66
Total	99.61	100.05	99.72	99.92	99.84	99.96	99.88
Ga	26.30	25.10	35.10	25.40	28.60	25.50	24.70
Rb	205.70	277.70	130.50	305.10	290.60	295.90	225.10
Sr	94.60	354.60	221.70	303.30	257.30	373.20	737.60
Y	1.00	4.40	0.90	1.50	1.20	11.40	2.50
Zr	812.20	235.30	729.70	452.00	464.80	222.10	377.50

Table 4. (Continued).

Nb	79.10	34.10	88.40	49.00	47.90	25.30	35.80
Ba	136.00	117.70	135.20	157.30	182.20	308.40	641.80
Ce	291.00	199.20	391.10	248.40	143.90	173.60	244.90
Hf	13.10	2.90	9.40	8.60	8.90	5.50	7.90
Ta	8.40	3.90	4.30	2.90	2.80	3.30	2.90
Th	25.50	88.10	47.40	103.50	67.40	43.50	75.80

Table 4. (Continued).

Sample no.	Medium crystalline nepheline syenite						
	BUZ-50	BUZ-51	BUZ-52	BUZ-55	BUZ-31	BUZ-32	BUZ-35
SiO_2	59.04	63.74	60.40	65.49	59.55	60.13	56.23
Al_2O_3	24.32	14.08	14.36	17.37	21.47	20.47	23.74
Fe_2O_3	1.35	4.29	3.83	1.79	1.03	1.22	0.74
MgO	0.06	1.20	1.43	0.02	0.03	0.05	0.02
MnO	0.10	0.21	0.16	0.07	0.10	0.12	0.02
Na_2O	4.53	4.66	3.99	5.71	10.58	8.73	12.90
K_2O	6.85	5.62	5.08	7.66	5.00	6.92	4.20
CaO	1.58	5.03	4.73	1.26	1.09	1.47	1.36
TiO_2	0.07	0.47	0.47	0.09	0.07	0.09	0.02
LOI	1.87	0.45	4.88	0.44	1.00	0.62	0.59
Total	99.83	99.98	99.52	99.98	99.96	99.93	99.89
Ga	32.40	20.90	21.80	23.80	34.90	30.60	41.30
Rb	290.90	257.80	208.80	317.40	371.90	468.70	285.70
Sr	139.80	527.10	558.30	96.80	268.50	339.10	112.50
Y	1.20	19.80	16.10	5.80	1.30	1.40	1.10
Zr	569.60	325.10	220.60	325.10	18.70	45.20	145.50
Nb	145.90	50.70	30.50	15.80	32.40	56.10	79.00
Ba	235.70	737.30	722.60	80.10	27.00	37.20	28.60
Ce	79.40	272.90	195.30	180.30	151.60	141.60	99.30
Hf	8.00	3.60	8.30	3.30	2.30	3.20	2.50
Ta	6.70	4.30	4.10	3.10	3.00	2.00	3.30
Th	53.10	40.70	36.20	146.90	13.60	15.80	6.00
Sample no.	Medium crystalline nepheline syenite						
	BUZ-36	BUZ-37	BUZ-38	BUZ-40	BUZ-42	BUZ-03	BUZ-04
SiO_2	59.39	60.84	58.55	57.00	60.30	64.86	61.88
Al_2O_3	21.55	20.35	21.47	15.47	20.98	17.66	20.93
Fe_2O_3	1.19	0.88	0.98	6.26	0.72	1.97	2.79
MgO	0.02	0.03	0.03	3.95	0.03	0.02	0.23
MnO	0.07	0.08	0.10	0.14	0.05	0.09	0.15
Na_2O	9.51	9.31	9.14	4.53	8.86	6.12	4.52
K_2O	6.28	5.65	6.04	2.22	6.62	6.79	6.88

Table 4. (Continued).

CaO	1.09	1.81	1.94	8.89	1.64	1.61	0.50
TiO_2	0.05	0.06	0.07	0.45	0.04	0.14	0.26
LOI	0.74	0.90	1.50	0.79	0.60	0.61	1.46
Total	99.98	99.92	99.85	99.95	99.87	99.99	99.74
Ga	33.90	30.20	37.70	20.60	28.40	23.90	27.90
Rb	400.50	372.70	444.10	161.60	369.00	279.70	367.40
Sr	337.10	294.00	212.90	428.70	339.80	348.70	481.00
Y	1.30	1.30	1.30	23.70	1.30	1.20	6.20
Zr	101.70	34.90	357.50	159.50	51.40	295.80	486.30
Nb	41.90	46.10	32.30	19.20	31.40	12.70	61.90
Ba	26.80	47.40	46.20	364.20	47.50	213.60	797.40
Ce	168.20	188.60	42.90	89.00	176.80	311.80	528.80
Hf	3.10	2.20	3.90	3.50	2.70	4.60	9.40
Ta	2.60	2.70	2.40	4.10	2.90	3.30	4.40
Th	15.40	12.70	2.10	10.00	11.90	105.20	93.70

Table 4. (Continued).

Sample no.	Coarse crystalline nepheline syenite						
	BUZ-80	BUZ-81	BUZ-83	BUZ-84	BUZ-85	BUZ-86	BUZ-87
SiO_2	64.54	64.09	63.98	64.17	63.95	54.23	58.74
Al_2O_3	17.66	17.12	17.75	17.33	17.03	23.60	24.90
Fe_2O_3	1.61	1.89	1.88	1.95	2.20	1.82	1.59
MgO	0.26	0.37	0.29	0.43	0.19	0.21	0.33
MnO	0.06	0.07	0.08	0.06	0.07	0.08	0.12
Na_2O	5.81	5.76	4.32	5.06	4.58	1.93	3.56
K_2O	6.78	6.93	7.27	7.64	8.05	9.06	8.48
CaO	2.15	2.55	2.88	1.87	2.65	4.58	0.17
TiO_2	0.12	0.11	0.11	0.14	0.14	0.10	0.07
LOI	0.67	0.85	0.94	0.85	0.75	3.52	1.66
Total	99.94	99.93	99.81	99.83	100.00	99.18	99.87
Ga	21.70	22.50	21.80	20.10	20.30	22.80	26.90
Rb	258.10	242.00	244.90	247.30	275.00	331.00	325.70
Sr	917.60	1005.00	1102.00	887.50	1036.00	478.60	343.10
Y	3.20	3.70	7.10	8.10	27.90	1.20	1.00
Zr	142.80	407.50	250.80	204.60	247.50	207.60	222.20
Nb	28.50	23.30	29.80	25.20	20.50	20.10	18.80
Ba	1042.00	1370.00	1387.00	1419.00	1132.00	974.20	718.80
Ce	48.70	156.70	170.50	181.90	133.50	298.30	528.40
Hf	2.50	2.90	3.60	5.10	3.40	3.60	5.90
Ta	3.20	3.10	3.00	2.90	3.60	3.20	3.00
Th	21.40	41.50	47.60	23.60	24.20	38.80	69.70

Table 4. (Continued).

Sample no.	Coarse crystalline nepheline syenite						
	BUZ-88	BUZ-89	BUZ-90	BUZ-91	BUZ-92	BUZ-09	BUZ-109
SiO_2	59.04	58.31	58.12	57.19	64.62	62.68	65.17
Al_2O_3	25.64	24.37	25.26	26.48	17.14	15.69	17.19
Fe_2O_3	0.92	1.82	2.25	1.72	1.75	4.60	1.98
MgO	0.26	0.25	0.17	0.25	0.34	0.03	0.19
MnO	0.02	0.13	0.15	0.03	0.06	0.20	0.06
Na_2O	3.23	2.62	3.12	2.69	4.95	5.52	5.21
K_2O	8.92	9.50	8.35	9.05	7.43	6.14	7.34
CaO	0.10	0.15	0.19	0.18	2.07	3.92	1.55
TiO_2	0.11	0.09	0.15	0.10	0.11	0.33	0.23
LOI	1.59	2.20	1.94	2.00	1.22	0.64	0.76
Total	99.85	99.57	99.79	99.78	99.98	99.94	99.88
Ga	25.00	21.80	27.50	23.90	19.30	24.80	19.60
Rb	333.70	331.30	312.80	336.90	266.20	294.60	283.40
Sr	316.00	355.70	549.30	412.80	867.80	280.80	480.80
Y	1.20	2.80	1.30	3.10	15.50	15.40	1.20
Zr	239.50	200.90	257.20	111.30	286.10	670.00	242.20
Nb	21.50	17.70	31.10	8.00	22.60	24.80	46.60
Ba	743.10	982.90	833.20	680.20	1171.00	275.80	407.60
Ce	65.50	505.50	178.90	403.70	243.90	705.10	502.10
Hf	6.50	8.50	6.90	2.50	5.70	11.30	4.30
Ta	2.80	5.20	2.80	2.80	3.50	4.10	2.80
Th	49.70	56.70	63.60	78.70	49.40	140.60	136.50

be derived from water deficiency in the magma, which was modified with the slab-derived fluids as a result of intruding into low- to medium-grade dehydrated crustal metamorphic rocks.

5.4. Tectonic discrimination

Boztuğ (1998) assessed postcollision uplift to late orogenic trends using major element geotectonic discrimination diagrams and within-plate granitoid geodynamic settings (İlbeyli et al., 2004) for Kırşehir region silica-oversaturated and -undersaturated alkaline plutons.

Eby (1992) divided A-type magmatism into two chemical groups. When we plot the Buzlukdağ samples on the Nb–Y–3Ga and Nb–Y–3Th trace element triangular diagrams, all the syenites plot on the A1 field, which were interpreted as differentiates of basalt magma derived from an ocean island basalt (OIB)-like source (Figure 12). The other alkaline plutons mainly plot in the same area. A1 is characterized by element ratios similar to OIBs and emplaced during intraplate magmatism, whereas the A2 group was derived from the subcontinental lithosphere or lower crust and emplaced in a postcollisional, postorogenic setting. The presence of a minor amount of quartz and variation of Th/Y versus Nb/Y suggest a slight enrichment of the crustal component within the main intrusive body (Figure 13).

The geochemical features of syenites suggest that the foid-bearing syenites are most closely associated with within-plate characteristics, so the Hf–Rb/10–Ta*3 triangular diagram (Figure 14) was used, which allowed distinction of the volcanic arc and within-plate affinity. In this diagram, the Buzlukdağ syenites and the other alkaline plutons plot on the intersection of the volcanic arc and within-plate field (Figure 14) (Harris et al., 1986). According to tectonic discrimination diagrams and the estimated emplacement depth of these rocks, the crustal thinning after the closure of the IT Ocean are the reason for derivation of these rocks rather than the postcollisional setting with crustal thickening in the region.

5.5. Geodynamic interpretation

Turkey is an important segment within the Alpine–Himalayan orogeny and comprises a number of continental blocks that are divided with suture zones derived from

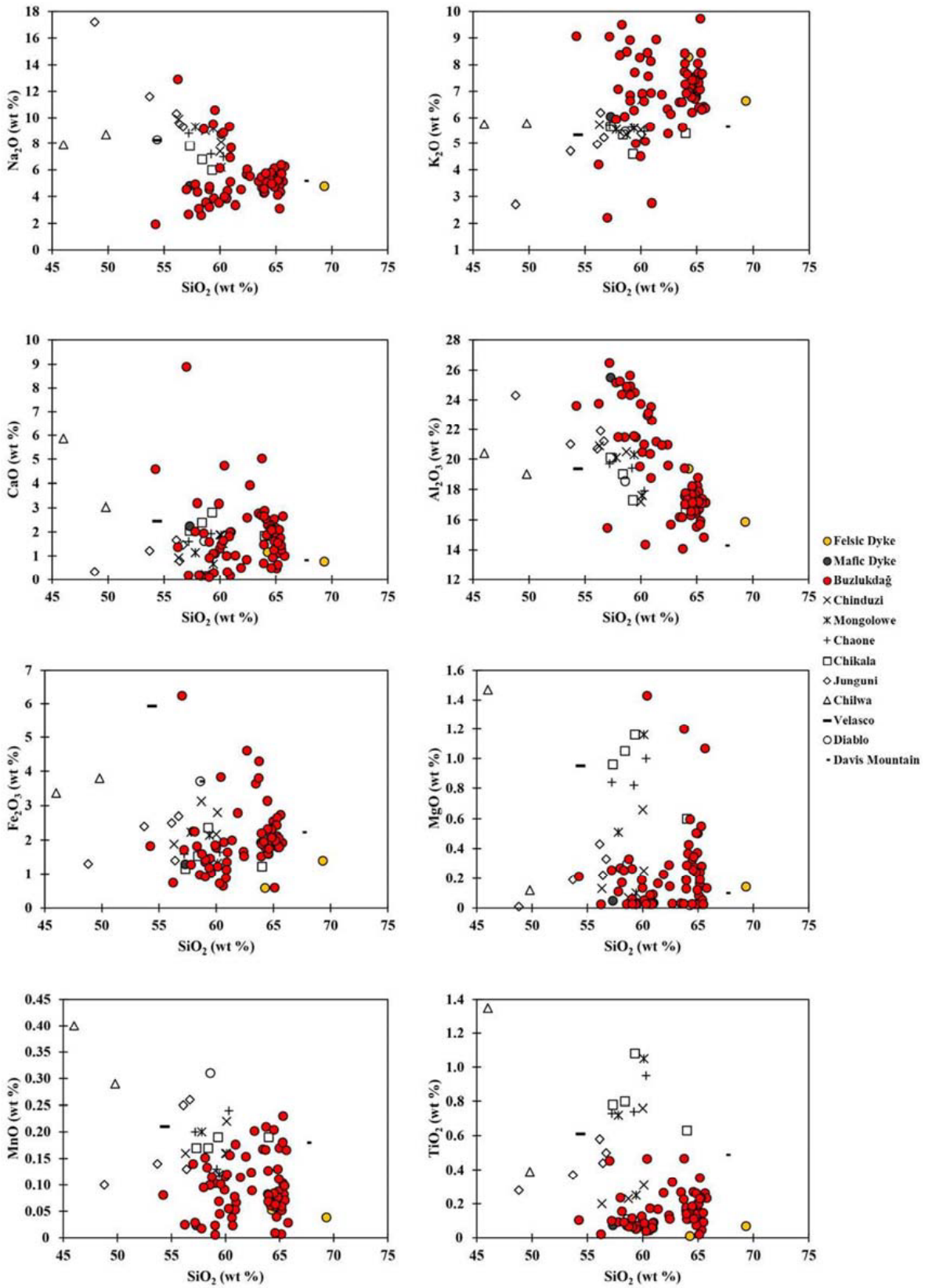

Figure 7. Harker variation diagrams of the Buzlukdağ Intrusive Complex (Harker, 1909). Data for other alkaline igneous rocks were taken from Fitton and Upton (1987).

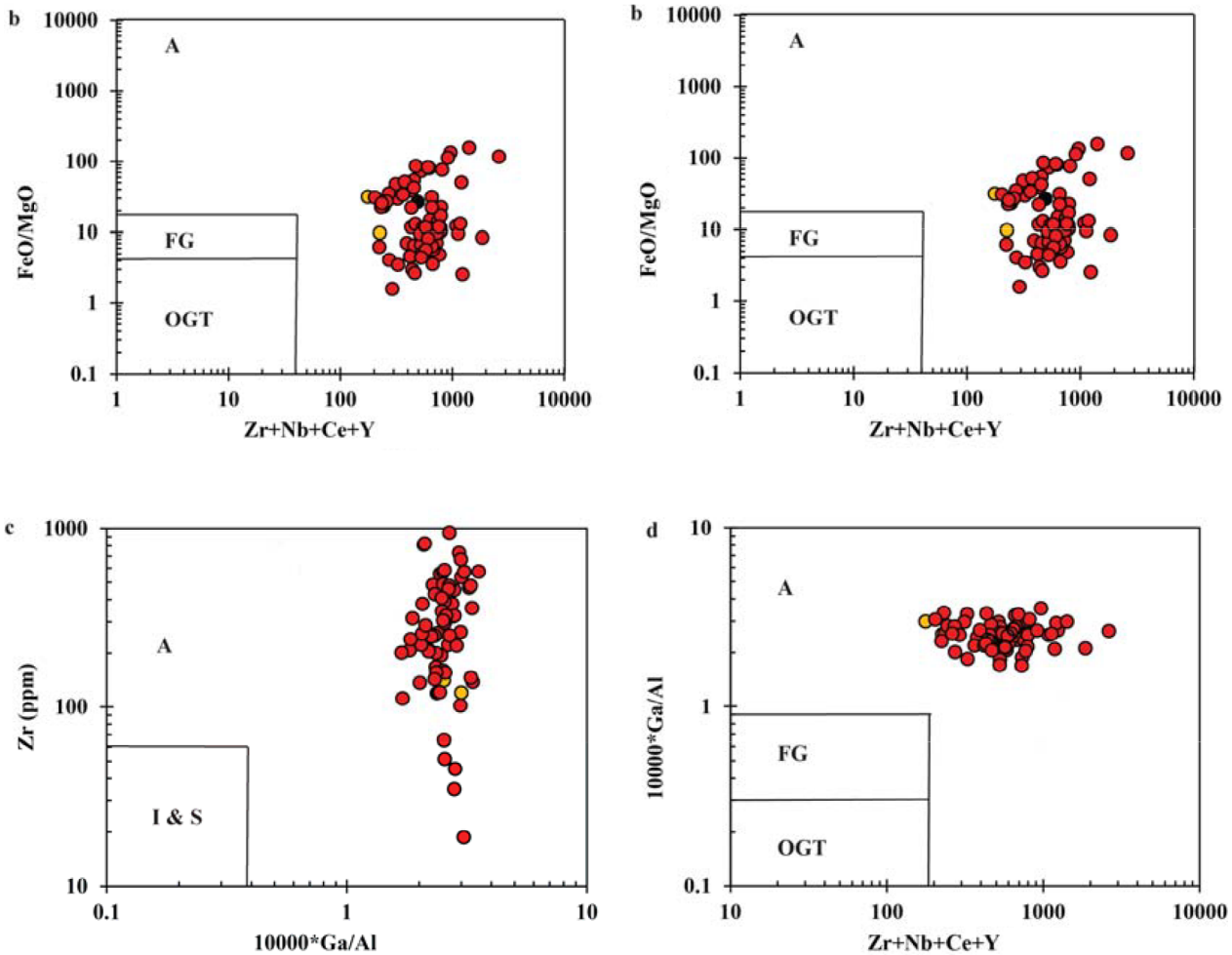

Figure 8. Classification of granite type after Whalen et al. (1987). (a) Zr + Nb + Ce + Y versus (%) $Na_2O + K_2O + CaO$, (b) Zr + Nb + Ce + Y versus (%) FeO/MgO, (c) 10000*Ga/Al versus Zr, (d) Zr + Nb + Ce + Y versus 10000*Ga/Al classification diagram (OGT: field for I–S and M-type granitoids, FC: field for fractionated I-type granitoids, A: A-type granitoids). The symbol descriptions are given in Figure 7.

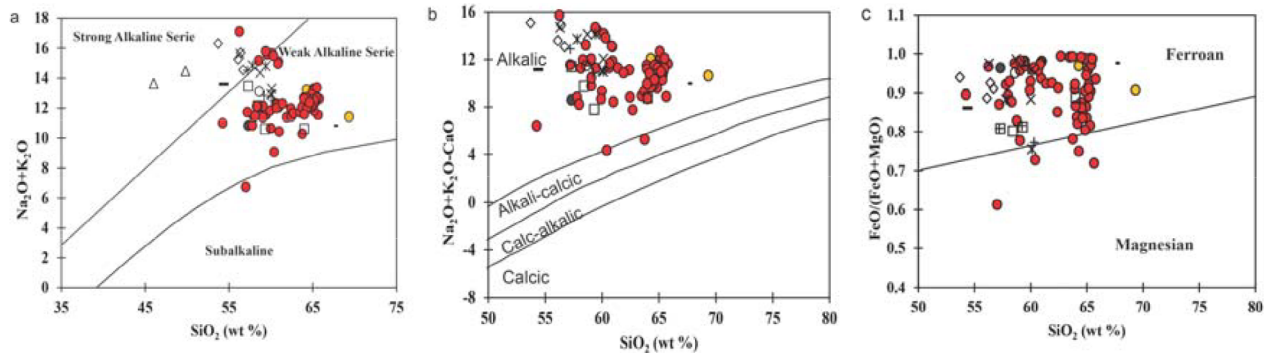

Figure 9. (a) SiO_2 versus total alkali, (b) $Na_2O + K_2O$ – CaO, and (c) FeO / (FeO + MgO) discrimination diagrams of the magmatic rock groups (Irvine and Baragar, 1971; Scharzer and Rogers, 1974; Frost et al., 2001). The symbol descriptions are given in Figure 7.

the closure of northern branches of the Neotethys Ocean (Şengör and Yılmaz, 1981). The closure of the Neotethys Ocean, which started in the Cenomanian–Turonian (95–90 Ma) (Garkunfel, 2004), was induced from calc-alkaline through alkaline magmatism within the CACC during the Late Cretaceous–Early Paleogene.

Table 5. Rare earth element (REE) compositions (ppm) of the Buzlukdağ syenitoids.

Sample no.	Coarse crystalline nepheline syenite				Medium crystalline nepheline syenite			
	BUZ-84	BUZ-109	BUZ-44	BUZ-77	BUZ-37	BUZ-114	BUZ-95	BUZ-05
La	82.40	211.30	50.50	41.00	82.90	209.20	85.50	287.10
Ce	149.10	436.30	97.50	78.30	121.30	281.00	150.10	492.80
Pr	14.07	33.32	9.94	7.80	8.56	17.29	16.41	37.24
Nd	44.90	83.00	35.30	25.20	17.70	31.80	52.70	86.60
Sm	5.49	4.08	5.06	2.47	0.79	1.03	4.18	3.83
Eu	1.11	0.47	1.11	0.52	0.09	0.11	0.70	0.45
Gd	3.05	0.05	3.27	0.85	0.05	0.05	1.16	0.05
Tb	0.50	0.10	0.49	0.14	0.02	0.02	0.19	0.15
Dy	2.47	0.34	2.42	0.58	0.07	0.10	0.91	0.76
Ho	0.40	0.04	0.45	0.09	0.02	0.02	0.13	0.12
Er	1.20	0.15	1.33	0.28	0.04	0.05	0.38	0.40
Tm	0.18	0.03	0.22	0.04	0.01	0.01	0.07	0.06
Yb	1.23	0.17	1.45	0.27	0.05	0.05	0.46	0.36
Lu	0.17	0.03	0.23	0.04	0.01	0.01	0.07	0.05
Y	13.90	2.90	15.90	3.20	0.50	0.60	5.60	4.50
Sample no.			Fine crystalline nepheline syenite					
	BUZ-93	BUZ-53	BUZ-16	BUZ-49	BUZ-23	BUZ-28	BUZ-26	
La	36.90	155.50	146.30	122.90	108.10	144.60	94.00	
Ce	68.10	322.50	264.20	197.30	225.40	256.00	160.20	
Pr	6.76	26.04	21.33	16.87	19.84	21.86	13.89	
Nd	21.40	67.80	54.10	52.30	66.00	62.00	43.40	
Sm	1.94	4.34	3.25	6.30	7.66	5.15	4.85	
Eu	0.38	0.43	0.44	1.35	1.20	0.86	0.85	
Gd	0.76	0.40	0.60	4.00	4.15	1.67	2.42	
Tb	0.14	0.15	0.13	0.63	0.65	0.27	0.39	
Dy	0.69	0.62	0.56	3.00	3.11	1.16	1.89	
Ho	0.14	0.10	0.07	0.55	0.53	0.14	0.32	
Er	0.40	0.33	0.20	1.75	1.71	0.40	0.97	
Tm	0.06	0.06	0.02	0.29	0.28	0.07	0.16	
Yb	0.42	0.46	0.16	1.92	1.81	0.38	1.03	
Lu	0.07	0.07	0.02	0.28	0.27	0.05	0.15	
Y	5.00	5.40	2.90	19.70	20.80	5.80	12.40	

There is no agreement on the geodynamic model for the evolution of Central Anatolian magmatism; some proposed models have already been explained. According to field observations, mapping, and mineralogical, petrographic, and geochemical data, foid-bearing syenites and the dykes of the Buzlukdağ Intrusive Complex are derived from same magma source with the same FC history under the AFC process. Assimilated crustal contaminant originated from source enrichment, which is associated with the subduction zone and contamination during the ascent through the thinning crust. The type of wall rock may reflect the main reason for the effect of water content in magma and induced derivation of silica-undersaturated rocks. The Buzlukdağ Intrusive Complex is derived from the lithospheric mantle, which is metasomatized by subduction fluids with crustal assimilation. From these

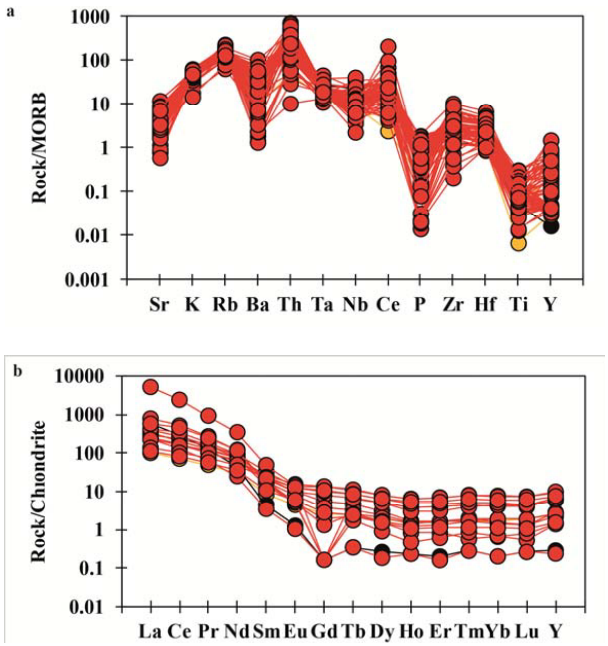

Figure 10. (a) MORB and (b) chondrite-normalized trace and rare earth element diagrams illustrating the geochemical characteristics of the Buzlukdağ Intrusive Complex. The chondrite and MORB normalization values are from Evensen et al. (1978) and Pearce et al. (1984), respectively. The symbol descriptions are given in Figure 7.

results, we can reconstruct a geodynamic model for the evolution of the Buzlukdağ intrusion.

No matter how good the U–Pb age data from all types of intrusive rocks from the CACC might be, there are lots of radiometric and K–Ar–Ar ages and some Pb–Pb ages, especially from granitoids (Kadıoğlu et al., 2003, 2006; Boztuğ and Jonckheere, 2007; Boztuğ et al., 2007a, 2009). According to age data from the literature, the calc-alkaline through alkaline magmatism in the CACC ranges from Upper Cretaceous to Lower Tertiary and this time interval, which is compatible with 30–50 Ma as suggested for the collision zone magmatism by Bonin (1990), is enough for the evolution of collision-related magmatic activity. The probable formation of Buzlukdağ alkaline intrusives can be explained with the illustrated tectonic model in Figures 15a–15d. In the Jurassic, the two oceans were left, which were closed with the İAE and IT suture zones. The CACC was bounded with these suture zones, from which its magmatism originated (Figure 15a). The magmatism resulted from either a N or NE dipping subduction zone. As suggested by Kadıoğlu et al. (2006), the magmatism might be related to the NE dipping subduction zone beneath the CACC and consumption of the oceanic lithosphere beneath the IT Basin during the Late Cretaceous. During the closure of the basin, melts of metasomatized upper mantle were injected to the upper crust, which initiated partial melting of calc-alkaline magmas (Kadıoğlu et al., 2003; İlbeyli et al., 2004) (Figure 15b). Rollback of the subducted plate, which was caused by the underplating of the buoyant continental crust of the Tauride platform, caused extension in the back-arc region (Figure 15c). The resultant lithospheric mantle upwelling into the thinned back-arc crust resulted in decompressional melting. The Buzlukdağ syenite probably resulted from the mixing of the asthenospheric mantle and subduction zone metasomatism mantle melts at this time, where the Buzlukdağ alkaline intrusives are generated by different

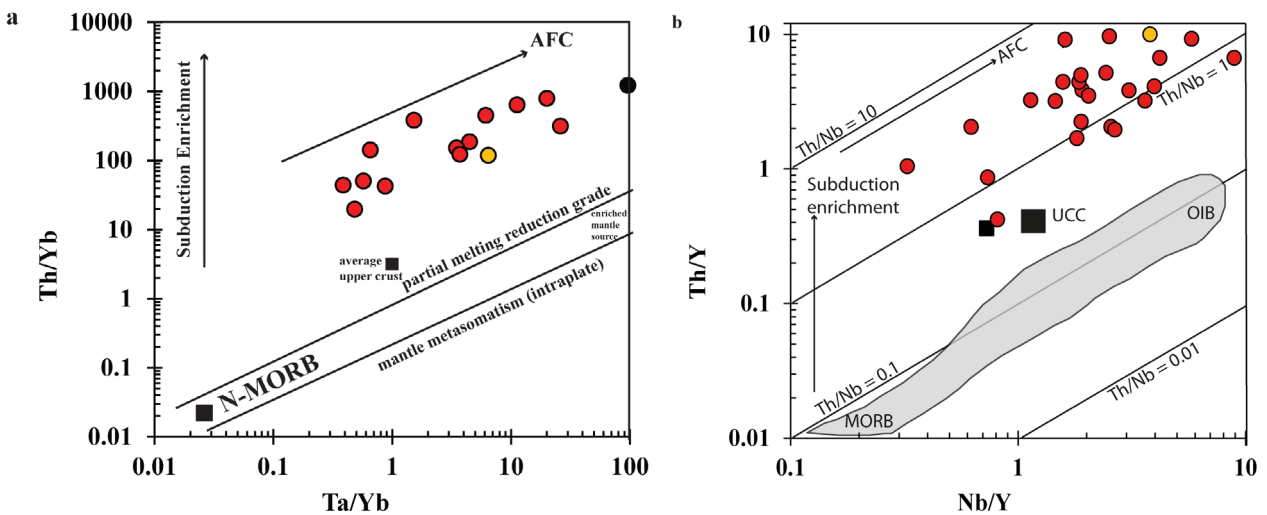

Figure 11. (a) log Ta/Yb versus log Th/Yb and (b) Th/Y versus Nb/Y diagram for the Buzlukdağ intrusives compared to the range of variation in mid-ocean ridge basalt (MORB) and ocean island basalt (OIB) (Pearce, 1983). Straight lines are contours of fixed Th/Nb ratio (AFC: assimilation fractional crystallization). The symbol descriptions are given in Figure 7.

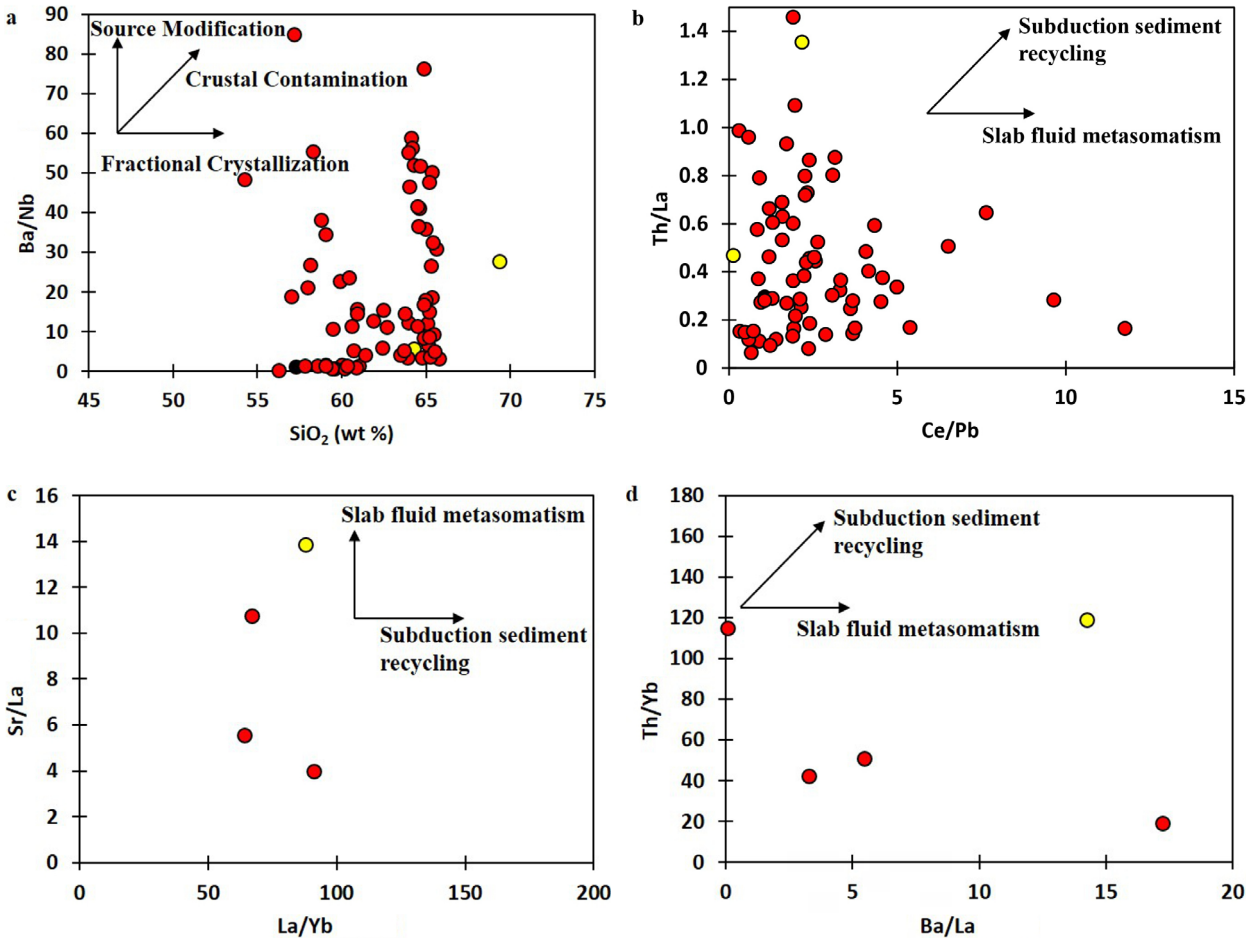

Figure 12. (a) SiO_2 versus Ba/Nb, (b) Ce/Pb versus Th/La, (c) La/Yb versus Sr/La, and (d) Ba/La versus Th/Yb diagrams of alkaline rocks within the CACC.

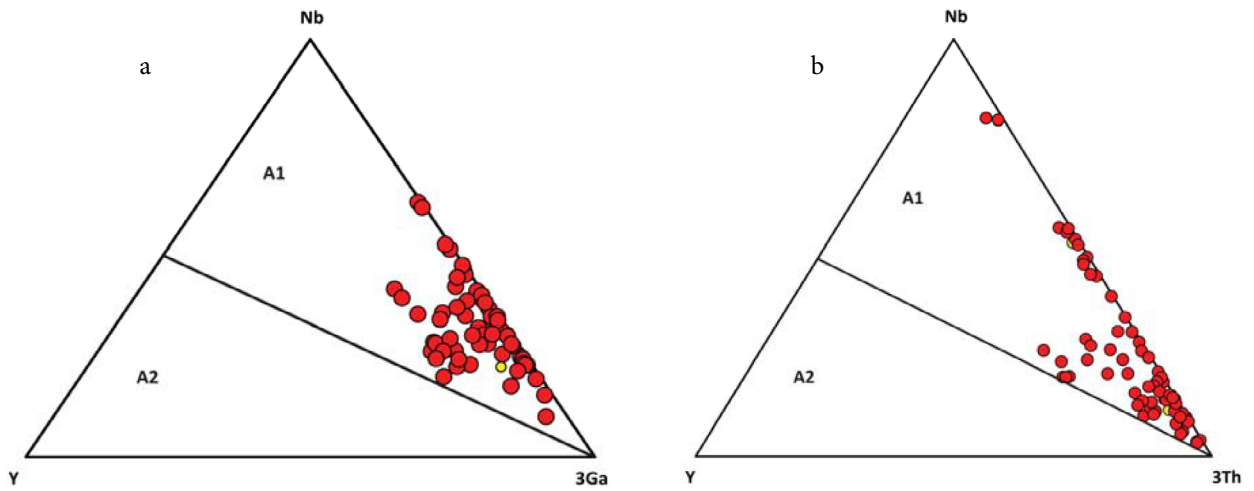

Figure 13. Discrimination diagrams of alkali granites [a) Nb–Y–3Ga and b) Nb–Y–3Th trace element triangle diagrams (Eby, 1992)] (A1: oceanic island basalts, A2: island arc basalts). The symbol descriptions are given in Figure 7.

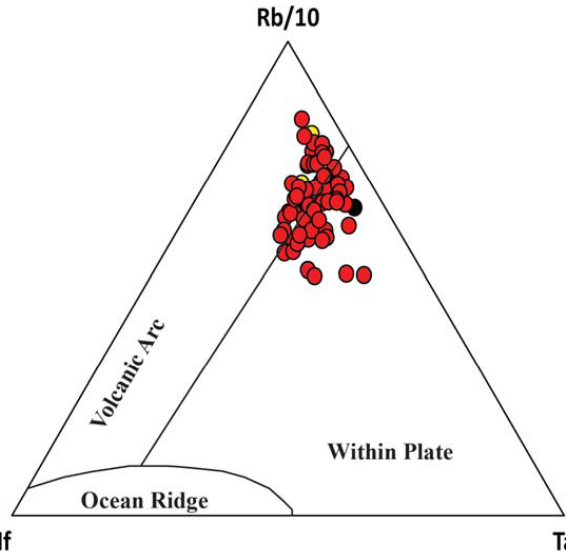

Figure 14. Tectonic discrimination diagram of Buzlukdağ syenitoids Hf–Rb/10–Ta*3 classification diagram (Harris et al., 1986). The symbol descriptions are given in Figure 7.

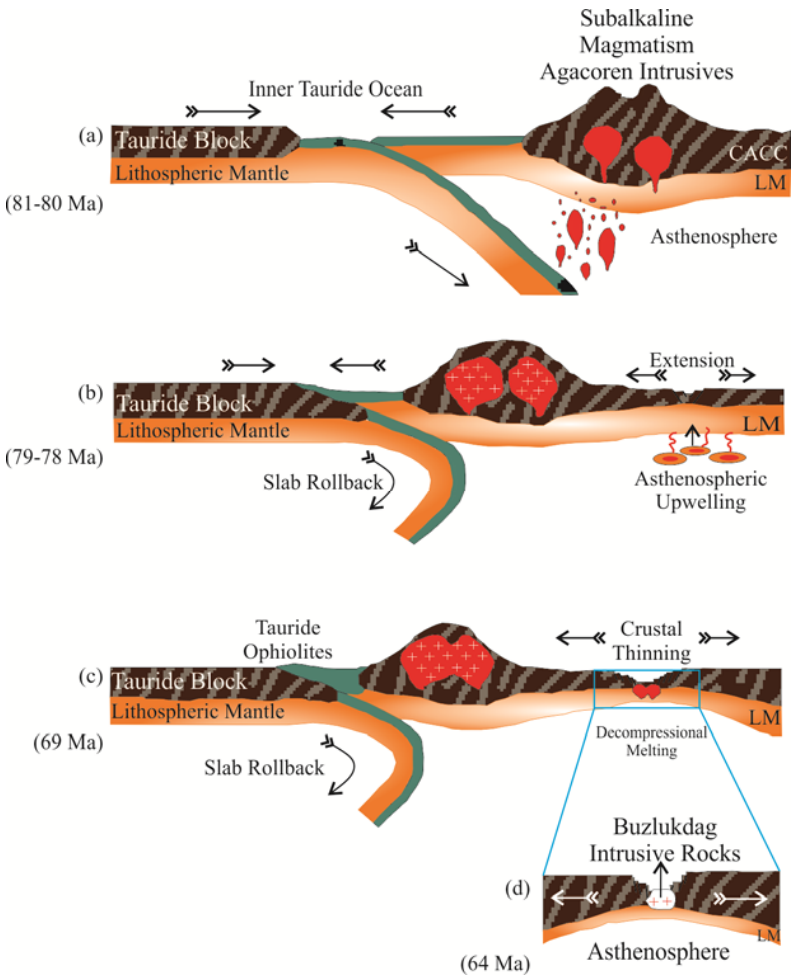

Figure 15. Tectonic model of Buzlukdağ intrusives in the CACC.

types and degrees of partial melting of the same mantle material and the type of the wall-rock that is assimilated during the ascent of the pluton also modifies the primary composition of the mantle that produced alkaline rocks (Figure 15d).

Acknowledgments
We gratefully acknowledge Ankara University BAP Project No. and DPT (2012K120440) for their support during the studies. We are also grateful to Fin Stuart for his comments that improved the paper.

References

Anderson JL (1996). Status of thermobarometry in granitic batholiths. T RSE Earth 87: 125-138.

Albaréde F (1996). Introduction to Geochemical Modeling. Cambridge, UK: Cambridge University Press.

Aydın NS, Göncüoğlu MC, Erler A (1998). Latest Cretaceous magmatism in the Central Anatolian Crystalline Complex: review of field, petrographic and geochemical features. Turkish J Earth Sci 7: 259-268.

Bayhan H (1988). Bayındır, Akpınar (Kaman) yöresindeki alkali kayaçların jeokimyası ve kökensel yorumu. Türkiye Jeoloji Kurumu Bülteni 31: 59-70 (in Turkish).

Bayhan H, Tolluoğlu AÜ (1987). Çayağzı siyenitoyidinin (Kırşehir kuzeybatısı) mineralojik-petrografik ve jeokimyasal özellikleri. Hacettepe Üniversitesi Yerbilimleri Dergi 14: 109-200 (in Turkish).

Bonin B (1987). Reflexions a propose de la repartition des granitoides les massifs cristallins externes des alpes françaises. Geologie Alpine 63: 137-149 (in French).

Bonin B (1988). From orogenic to anorogenic environments: evidence from associated magmatic episodes. Schweiz Mineral Petrogr Mitt 68: 301-311.

Bonin B (1990). From orogenic to anorogenic settings: evolution of granitoid suites after a major orogenesis. Geol J 25: 261-270.

Bozkurt E (2001). Neotectonics of Turkey–a synthesis. Geodin Acta 14: 3-30.

Bozkurt E, Mittwede SK (2001). Introduction to the geology of Turkey—a synthesis. Int Geol Rev 43: 578-594.

Boztuğ D (1998). Post-collisional central Anatolian alkaline plutonism, Turkey. Turkish J Earth Sci 7: 145-165.

Boztuğ D (2000). S–I–A–type intrusive associations: geodynamic significance of synchronism between metamorphism and magmatism in central Anatolia, Turkey. In: Bozkurt E, Winchester JA, Piper JDA, editors. Tectonics and Magmatism in Turkey and the Surrounding Area. London, UK: Geological Society of London Special Publications, pp. 441-458.

Boztuğ D, Arehart GB (2007). Oxygen and sulphur isotope geochemistry revealing a significant crustal signature in the genesis of the post–collisional granitoids in Central Anatolia, Turkey. J Asian Earth Sci 30: 403-416.

Boztuğ D, Güney Ö, Heizer M, Jonckheere RC, Tichomirowa M, Otlu N (2009). ^{207}Pb-^{206}Pb, ^{40}Ar-^{39}Ar and fission-track geothermochronology quantifying cooling and exhumation history of the Kaman-Kırşehir region intrusions, Central Anatolia, Turkey. Turkish J Earth Sci 18: 85-108.

Boztuğ D, Harlavan Y (2008). K-Ar ages of granitoids unravel the stages of Neo-Tethyan convergence in the eastern Pontides and Central Anatolia, Turkey. Int J Earth Sci 97: 585-599.

Boztuğ D, Harlavan Y, Arehart GB, Satır M, Avcı N (2007a). K–Ar age, whole-rock and isotope geochemistry of A-type granitoids in the Divriği–Sivas region, eastern-central Anatolia, Turkey. Lithos 97: 193-218.

Boztuğ D, Jonckheere RC (2007). Apatite fission track data from central Anatolian granitoids (Turkey): constraints on Neo-Tethyan closure. Tectonics 26: TC3011.

Boztuğ D, Tichomirowa, M, Bombach, K (2007b). ^{207}Pb-^{206}Pb single-zircon evaporation ages of some granitoid rocks reveal continent-oceanic island arc collision during the Cretaceous geodynamic evolution of the central Anatolian crust, Turkey. J Asian Earth Sci 31: 71-86.

Boztuğ D, Yılmaz S, Kesgin Y (1994). Petrography, petrochemistry and petrogenesis of the eastern part of Kösedağ pluton from the Central–Eastern Anatolian alkaline province, Suşehri, NE Sivas. Geological Bulletin of Turkey 32: 1-12 (in Turkish with English abstract).

Channel JET (1986). Palaeomagnetism and continental collision in the Alpine Belt and the formation of late-tectonic extensional basin. In: Coward MP, Ries AC, editors. Collision Tectonics. London, UK: Geological Society of London Special Publications, pp. 261-284.

Das M, Acharya S (1996). Petrochemical nature of Baranadağ alkaline igneous complex, Orissa, India. J Southeast Asian Earth Sci 14: 293-297.

Deer WA, Howie RA, Zussman J (1963). Rock-Forming Minerals. Volume 4, Framework Silicates. London, UK: Longmans.

Deniz K (2010). Geology, petrology and investigation of Buzlukdağı (Kırşehir) alkaline magmatic rocks through confocal Raman spectroscopy. MSc, Ankara University, Ankara, Turkey (in Turkish with English abstract).

Dilek Y, Altunkaynak Ş (2009). Geochemical and temporal evolution of Cenozoic magmatism in western Turkey: mantle response to collision, slab break-off, and lithospheric tearing in an orogenic belt. Geol Soc Spec Publ 311: 213-233.

Dilek Y, Altunkaynak Ş (2010). Geochemistry of Neogene–Quaternary alkaline volcanism in western Anatolia, Turkey, and implications for the Aegean mantle. Int Geol Rev 52: 631-655.

Eby GN (1992). Chemical subdivision of the A-type granitoids; petrogenetic and tectonic implications. Geology 20: 641-644.

Eby GN (2006). From carbonatites to alkali granites–Petrogenetic insights from the Chilwa and Monteregian Hills–White Mountain igneous provinces. In: Geological Association of Canada–Mineralogical Association of Canada Joint Annual Meeting, pp. 31-45.

Eby GN (2011). A-type granites: magma sources and their contribution to the growth of the continental crust. In: Seventh Hutton Symposium on Granites and Related Rocks, pp. 50-51.

Elburg MA, Bergen MV, Hoogewerff J, Foden J, Vroon P, Zulkarnain I, Nasution A (2002). Geochemical trends across an arc-continent collision zone: magma sources and slab-wedge transfer processes below the Pantar Strait volcanoes. Indonesia. Geochim Cosmochim Acta 66: 2771-2789.

Elitok Ö, Özdamar Ş, Bacak G, Baktaş U (2014). Geological, petrological and geodynamical characteristics of the Karacaali Magmatic Complex (Kırıkkale) in the Central Anatolian Crystalline Complex, Turkey. Turkish J Earth Sci 23: 645-667.

Ersoy Y, Helvacı C (2007). Stratigraphy and geochemical features of the Early Miocene bimodal (ultrapotassic and calc-alkaline) volcanic activity within the NE-trending Selendi Basin, Western Anatolia, Turkey. Turkish J Earth Sci 16: 117-139.

Ersoy Y, Helvacı C, Sözbilir H, Erkül F, Bozkurt E (2008). A geochemical approach to Neogene–Quaternary volcanic activity of western Anatolia: an example of episodic bimodal volcanism within the Selendi Basin, Turkey. Chem Geol 255: 265-282.

Ersoy EY, Helvacı C, Palmer MR (2010a). Mantle source characteristics and melting models for the early-middle Miocene mafic volcanism in Western Anatolia: Implications for enrichment processes of mantle lithosphere and origin of K–rich volcanism in post–collisional settings. J Volcanol Geoth Res 198: 112-128.

Ersoy YE, Helvacı C, Palmer MR (2011). Stratigraphic, structural and geochemical features of the NE–SW trending Neogene volcano-sedimentary basins in western Anatolia: Implications for associations of supra-detachment and transtensional strike-slip basin formation in extensional tectonic setting. J Asian Earth Sci 41: 159-183.

Ersoy YE, Helvacı C, Palmer MR (2012). Petrogenesis of the Neogene volcanic units in the NE–SW–trending basins in western Anatolia, Turkey. Contrib Mineral Petrol 163: 379-401.

Ersoy YE, Helvacı C, Sözbilir H (2010b). Tectono-stratigraphic evolution of the NE-SW-trending superimposed Selendi basin: implications for late Cenozoic crustal extension in Western Anatolia, Turkey. Tectonophysics 488: 210-232.

Evensen NM, Hamilton PJ, O'Nions RK (1978). Rare earth abundances in chondritic meteorites. Geochim Cosmochim Acta 42: 1199-1212.

Fitton JG, Upton BGJ, editors. (1987). Alkaline igneous rocks. London, UK: Geological Society Special Publication.

Frost BR, Barnes CG, Collins WJ, Arculus RJ, Ellis DJ, Frost CD (2001). A geochemical classification for granitic rocks. J Petrol 42: 2033-2048.

Garfunkel Z (2004). Origin of the eastern Mediterranean basin: a re-evaluation. Tectonophysics 391: 11-34.

Göncüoğlu MC, Köksal S, Floyd PA (1997). Post-collisional A-type magmatism in the Central Anatolian Crystalline Complex: petrology of the İdiş Dağı intrusives (Avanos, Turkey). Turkish J Earth Sci 6: 65-76.

Harker A (1909). Metamorphism, A Study of the Transformation of Rock Mases. London, UK: Methuen.

Harris NBW, Pearce JA, Tindle AG (1986). Geochemical characteristics of collision-zone magmatism. In: Coward MP, Riesi AC, editors. Collision Tectonics. London, UK: Geological Society of London Special Publication, pp. 67-68.

Hawkesworth CJ, Turner SP, McDermott F, Peate DW, Van Calsteren P (1997). U–Th isotopes in arc magmas: implications for element transfer from the subducted crust. Science 276: 551-555.

Hess HH (1941). Pyroxenes of common mafic magmas. Am Mineral 26: 515-535.

Holland T, Blundy J (1994). Non-ideal interactions in calcic amphiboles and their bearing on amphibole-plagioclase thermometry. Contrib Mineral Petrol 116: 433-447.

İlbeyli N (1999). Petrogenesis of collision related plutonic rocks, Central Anatolia (Turkey). PhD, University of Durham, Durham, UK.

İlbeyli N (2005). Mineralogical-geochemical constraints on intrusives in Central Anatolia, Turkey: tectono-magmatic evolution and characteristics of mantle source. Geol Mag 142: 187-207.

İlbeyli N, Pearce JA, Meighan IG, Fallick A (2009). Contemporaneous Late Cretaceous calc-alkaline and alkaline magmatism in Central Anatolia, Turkey: oxygen isotope constraints on petrogenesis. Turkish J Earth Sci 18: 529-547.

İlbeyli N, Pearce JA, Thirlwall MF, Mitchell JG (2004). Petrogenesis of collision-related plutonics in Central Anatolia, Turkey. Lithos 72: 163-182.

Irvine TN, Baragar WRA (1971). A guide to the chemical classification of the common volcanic rocks. Canadian J Earth Sci 8: 523-548.

Kadıoğlu YK, Dilek Y, Foland KA (2006). Slab break-off and syncollisional origin of the Late Cretaceous magmatism in the Central Anatolian Crystalline Complex. Geol S Am S 409: 381-415.

Kadıoğlu YK, Dilek Y, Güleç N, Foland KA (2003). Tectonomagmatic evolution of bimodal plutons in the Central Anatolian Crystalline Complex, Turkey. J Geol 111: 671–690.

Kadıoğlu YK, Güleç N (1996). Mafic microgranular enclaves and interaction between felsic and mafic magmas in the Ağaçören Intrusive Suite: evidence from petrographic features and mineral chemistry. Int Geol Rev 38: 854-867.

Kadıoğlu YK, Güleç N (1999). Types and genesis of the enclaves in central Anatolian granitoids. Geol J 34: 243-256.

Kadıoğlu YK, Üstündağ Z, Deniz K, Yenikaya C, Erdoğan Y (2009). XRF and Raman characterization of antimonite. Instrum Sci Technol 37: 683-696.

Karsli O, Caran Ş, Dokuz A, Çoban H, Chen B, Kandemir R (2012). A-type granitoids from the Eastern Pontides, NE Turkey: records for generation of hybrid A-type rocks in a subduction-related environment. Tectonophysics 530-531: 208-224.

Keskin M (2003). Magma generation by slab steepening and breakoff beneath a subduction–accretion complex: an alternative model for collision-related volcanism in Eastern Anatolia, Turkey. Geophys Res Lett 30: 8046.

Koç Ş, Özmen Ö, Doğan AU (2003). Geochemistry of fluorite mineralization in Kaman, Kırşehir, Turkey. J Geol Soc India 62: 305-317.

Köksal S, Göncüoğlu MC (2008). Sr and Nd isotopic characteristics of some S-I and A-type granitoids from Central Anatolia. Turkish J Earth Sci 17: 111-127.

Köksal S, Göncüoğlu MC, Floyd PA (2001). Extrusive members of postcollisional A-type magmatism in Central Anatolia: Karahıdır Volcanics, İdişdağı–Avanos area, Turkey. Int Geol Rev 43: 683-691.

Köksal S, Moller A, Göncüoğlu CM, Frei D, Gerdes A (2012). Crustal homogenization revealed by U–Pb zircon ages and Hf isotope evidence from the Late Cretaceous granitoids of the Ağaçören intrusive suite (Central Anatolia/Turkey). Contrib Mineral Petrol 163: 725-743.

Köksal S, Romer RL, Göncüoğlu MC, Köksal FT (2004). Timing of post-collisional H-type to A-type granitic magmatism: U–Th titanite ages from the Alpine central Anatolian granitoids (Turkey). Int J Earth Sci 93: 974-989.

Koralay T (2010). Petrographic and geochemical characteristics of upper Miocene Tekkedag volcanics (Central Anatolia–Turkey). Chem Erde-Geochem 70: 335-351.

Koralay T, Kadıoğlu YK (2008). Reasons of different colors in the ignimbrite lithology: micro-XRF and confocal Raman spectrometry method. Spectrochim Acta A 69: 947-955.

Leake BE (1978). Nomenclature of amphiboles. Mineral Magazine 42: 533-563.

Lünel AT, Akıman O (1986). Pseudoleucite from Hamitköy area, Kaman, Kırşehir occurrence and its use as a pressure indicator. MTA Enst Dergisi 103-104: 117-23 (in Turkish with English abstract).

McKenzie DP, Bickle MJ (1988). The volume and composition of melt generated by extension of the lithosphere. J Petrol 29: 625-679.

Nelson ST, Davidson JP (1993). Interaction between mantle-derived magmas and mafic crust, Henry Mountains, Utah. J Geophys Res 98: 1837-1852.

Otlu N, Boztuğ D (1998). The coexistency of the silica oversaturated (alkos) and undersaturated alkaline (alkus) rocks in the Kortundağ and Baranadağ plutons from the Central Anatolian alkaline plutonism, E Kaman/NW Kırşehir, Turkey. Turkish J Earth Sci 7: 241-258.

Özdemir Y, Karaoğlu Ö, Tolluoğlu AÜ, Güleç N (2006). Volcanostratigraphy and petrogenesis of the Nemrut stratovolcano (East Anatolian High Plateau): the most recent post-collisional volcanism in Turkey. Chem Geol 226: 189-211.

Özkan HM, Erkan Y (1994). A petrological study on a foid syenite intrusion in central Anatolia (Kayseri-Turkey). Turkish J Earth Sci 3: 45-55.

Pearce JA (1983). Role of the sub-continental lithosphere in magma genesis at active continental margins. In: Hawkesworth CJ, Norry MJ, editors. Continental Basalts and Mantle Xenoliths. Nantwich, UK: Shiva, pp. 230-249.

Pearce JA, Harris NBW, Tindle AG (1984). Trace-element discrimination diagrams for the tectonic interpretation of granitic rocks. J Petrol 25: 956-983.

Pearce JA, Parkinson IJ (1993). Trace element models for mantle melting: application to volcanic arc petrogenesis. Geol Soc Spec Publ 76: 373-403.

Pearce JA, Peate DW (1995). Tectonic implications of the composition of volcanic ARC magmas. Annu Rev Earth Pl Sc 23: 251-285.

Rollinson HR (1993). Using Geochemical Data: Evaluation, Presentation, Interpretation. London, UK: Longman Scientific and Technical.

Scharzer RR, Rogers JJW (1974). A worldwide comparison of alkali olivine basalts and their differentiation trends. Earth Planet Sci Lett 23: 286-296.

Şengör AMC, Yılmaz Y (1981). Tethyan evolution of Turkey: a plate tectonic approach. Tectonophysics 75: 181-241.

Seymen I (1981). Stratigraphy and metamorphism of the Kırşehir Massif around Kaman (Kırşehir–Turkey). Bulletin of the Geological Society of Turkey 24: 7-14.

Streckeisen A (1976). To each plutonic rock its proper name. Earth Sci Rev 12: 1-33.

Streckeisen A (1979). Classification and nomenclature of volcanic rocks: its proper name. Earth Sci Rev 12: 1-33.

Tarhan N (1985). Doğu Toroslar'da, Neo-tetis'in Kapanımına İlişkin Granitoyid Magmaların Evrimi ve Kökeni. MTA Dergisi: 95-113 (in Turkish).

Tatar S (2003). Behrekdağ batoliti'nin Kırıkkale İli–Hirfanlı Barajı arasında kuzey–güney yönlü bir jeotravers boyunca petrolojik incelemesi. PhD, Cumhuriyet University, Sivas, Turkey (in Turkish).

Tatar S, Boztuğ D (1998). Fractional crystallization and magma mingling/mixing processes in the monzonitic association in the SW part of the composite Yozgat batholith (Şefaatli–Yerköy, SW Yozgat). Turkish J Earth Sci 7: 215-230.

Tatar S, Boztuğ D (2005). The syn-collisional Danacıobası biotite leucogranite derived from the crustal thickening in central Anatolia (Kırıkkale), Turkey. Geol J 40: 571-591.

Temizel İ, Arslan M (2008). Petrology and geochemistry of Tertiary volcanic rocks from the Ikizce (Ordu) area, NE Turkey: implications for the evolution of the eastern Pontide paleo-magmatic arc. J Asian Earth Sci 31: 439-463.

Temizel İ, Arslan M (2009). Mineral chemistry and petrochemistry of post-collisional Tertiary mafic to felsic cogenetic volcanics in the Ulubey (Ordu) Area, Eastern Pontides, NE Turkey. Turkish J Earth Sci 18: 29-53.

Temizel İ, Arslan M, Ruffet G, Peucat JJ (2012). Petrochemistry, geochronology and Sr–Nd isotopic systematics of the Tertiary collisional and post-collisional volcanic rocks from the Ulubey (Ordu) area, eastern Pontide, NE Turkey: implications for extension-related origin and mantle source characteristics. Lithos 128: 126-147.

Thompson RN, Morrison MA, Hendry GL, Parry SJ (1984). An assessment of the relative roles of a crust and mantle in magma genesis: an elemental approach. Philos T Roy Soc A 310: 549-590.

Tolluoğlu AÜ (1986). Orta Anadolu Masifinin güneybatısında (Kırşehir yöresinde) petrografik ve petrotektonik incelemeler. PhD, Hacettepe University, Ankara, Turkey (in Turkish).

Tolluoğlu AÜ (1993). Kırşehir Masifini kesen felsik intrüziflerin (Kötüdağ ve Buzlukdağ) petrografik ve jeokimyasal karakterleri. Yerbilimleri 16: 19-43 (in Turkish).

Wang A, Freeman J, Kuebler KE (2002). Raman spectroscopic characterization of phyllosilicates. In: Lunar and Planetary Science XXXIII, p. 1374.

Whalen JB, Currie KL, Chappell BW (1987). A-type granites: geochemical characteristics, discrimination and petrogenesis. Contrib Mineral Petrol 95: 407-419.

Whitney DL, Teyssier C, Dilek Y, Fayon AK (2001). Metamorphism of the Central Anatolian Crystalline Complex, Turkey: influence of orogen-normal collision vs. wrench-dominated tectonics on P–T–t paths. J Metamorph Geol 19: 411-432.

Wilson M (1989). Igneous Petrogenesis. London, UK: Unwin Hyman.

Woolley AR, Jones GC (1987). The Petrochemistry of the Northern Part of the Chilwa Alkaline Province, Malawi. London, UK: Geological Society Special Publication.

Yılmaz S, Boztuğ D (1994). Granitoyid petrojenezinde magma mingling/mixing kavramı: Türkiye'den bazı örnekler. Jeoloji Mühendisliği 44-45: 1-20 (in Turkish).

Yılmaz Şahin S, Boztuğ D (2001). Magma karışması (magma mingling/mixing). In: Boztuğ D, Otlu N, editors. Magmatik Petrojenez, TÜBİTAK Lisansüstü Yaz Okulu. Ankara, Turkey: TÜBİTAK, pp. 543-579.

Zellmer GF, Annen C, Charlier BLA, George RMM, Turner SP, Hawkesworth CJ (2005). Magma evolution and ascent at volcanic arcs: constraining petrogenetic processes through rates and chronologies. J Volcanol Geotherm Res 140: 171-191.

Zozulya DR, Eby GN (2008). The anorthosite - A-type peralkaline granite connection: a case study from the Keivy Terrane, Baltic Shield. In: Geological Association of Canada and Mineralogical Association of Canada, Joint Annual Meeting, pp. 190–191.